

1
2
3
4
5
6
7
8
9
10
11
12
13
14
15

Inter-model variability and mechanism attribution of central and southeastern U.S. anomalous cooling in the 20th century as simulated by CMIP5 models

Zaitao Pan,¹Xiaodong Liu,²Sanjiv Kumar³, Zhiqiu Gao,⁴ and James Kinter³

- 1: Saint Louis University, St. Louis, MO 63108, USA
- 2: Institute of Earth Environment, Chinese Academy of Sciences, Xi'an, Shaanxi, 710075, China
- 3: Center for Ocean-Land-Atmosphere Studies, 4041 Powder Mill Road, Suite 302, Calverton, MD, 20705, USA
- 4: Institute of Atmospheric Physics, Chinese Academy of Sciences, Beijing, 100029, China

Submitted to J. Climate
31 July, 2012

Abstract

Many parts of the central and southeastern U.S. cooled by up to 2 °C during the 20th century, while global mean temperature rose by 0.6 °C (0.76 °C from 1901-2006). Although other regions such as central China and central South America also experienced a cooling trend, the so-called “warming hole (WH)”, the cooling is much weaker than in the U.S. WH. Studies have shown that the Pacific Decadal Oscillation (PDO) and the Atlantic Multidecadal Oscillation (AMO) may be responsible for this cooling, while other works reported that regional scale processes like the low-level jet and evapotranspiration contribute to the abnormality. Only a few of 53 simulations by CMIP3 (phase 3 of the Coupled Model Intercomparison Project) models could reproduce the cooling. This study analyzes newly available simulations in CMIP5 (phase 5 of CMIP) experiments from 27 models, totaling 173 ensemble members. We found that (i) the observed cooling occurred largely in the southeastern U.S. in the 3rd quarter and central U.S. in the 4th quarter of the 20th century, (ii) while a large number of models have difficulty in reproducing the cooling, those with the highest resolutions tend to capture the WH-like summer cooling in the central U.S., (iii) the simulations with forcing only by greenhouse gases (GHG) produced strong warming in the central U.S. that may have compensated the cooling, and (iv) the all-forcing *historical* experiment compared with the natural-forcing-only experiment showed a well-defined WH in the central U.S., implying that land surface processes contributed to the cooling in the 20th century.

1. Introduction

The Earth's surface has experienced unprecedented warming since the Industrial Revolution began in the 1850s. The global mean surface air temperature over land rose 0.76°C during 1901-2006 (IPCC, 2007). This global warming has been neither spatially uniform nor persistent in time. The warming is faster in the high latitudes than in the tropics and greater in winter than summer, largely due to snowmelt-albedo feedbacks (Holland and Bitz, 2003). It is also widely reported that the nighttime temperature rose more than the daytime temperature because of cloud cover and other feedback processes (Karl et al., 1993). Furthermore, high mountain regions warmed more than low-lying regions (Liu and Chen, 2000).

The above general features are well-documented, robust features of climate warming. On regional scales, temperature changes often deviate from these patterns. There are some special geographical regions where a lack of warming or even a cooling has occurred. The central and southeastern U.S. (CSE) actually cooled in the 20th century, most notably during the second half of the century, while global mean temperature warmed at an increasing rate. The cooling or lack of warming regions is referred to as “warming holes (WHs)” (Pan et al., 2004; Kunkel et al., 2006). Attention has been paid to this abnormal cooling trend both observationally and in modeling (Tett et al., 2002; Portmann et al., 2009; Meehl et al., 2012). Kalnay and Cai (2003) have attributed this cooling trend to land surface processes by reconciling the temperature difference between upper-air and surface observations. Combining observations with a regional climate model's results, Pan et al., (2004) suggested that regional hydrological processes coupled with the low-level jet contribute to the cooling. Other studies have attributed the cooling to the internal dynamics (Kunkel et al., 2006; Liang, et al., 2006). A number of modeling studies have attributed the mechanisms for this abnormal trend to large-scale

decadal oscillations such as the Pacific Decadal Oscillation (PDO) and the Atlantic Multidecadal Oscillation (AMO) (Robinson et al., 2002; Kunkel et al., 2006; Wang et al., 2009; Meehl et al., 2012).

While seeking reasons why only this part of the U.S. experienced cooling, Pan et al. (2009) found other similar WHs: one in south-central China and the other in central South America. Some features common to these WHs are their presence (1) on the eastern slope of major mountain ranges where the climatic warming gradient exists, (2) at the low-level jet termini where warm-moist air converges, and (3) in intense agricultural regions where the deep crop roots can extract soil moisture.

The mid-continental cooling goes against the common belief that the middle of continents, far from oceans, should warm faster than coastal regions. Also, it was a challenge for the great majority of models in phase 3 of the Coupled Model Intercomparison Project (CMIP3) models to reproduce the WHs (Kunkel et al., 2006). It is of interest to see how well the phase 5 (CMIP5, Taylor et al., 2012) models reproduce WHs in the 20th century as well as how they predict their fate in the 21st century. The purposes of this paper are to (1) see how well CMIP5 models reproduce this abnormal cooling, (2) find what the common features of the models are that simulated WHs well or vice versa, and (3) determine what mechanisms are responsible for the WHs as simulated in the new generation of the atmosphere-ocean coupled general circulation models (AOGCMs). A companion paper (Kumar et al. 2012) investigates other aspects of the WH trends in North America. More general results regarding North American climate are reported in Sheffield et al. (2012a and 2012b) and Maloney et al. (2012).

64

65

66 **2. Model and data**

67 The design of CMIP5 includes the new short-term decadal experiments hindcasting the interannual variability, emission(versus
68 concentration) driven Earth system model (ESM) simulations exploring the sensitivity of the carbon cycle feedback, and time-
69 evolving land use runs allowing for the dynamic vegetation feedback (Taylor et al., 2012). The core long-term CMIP5 simulations
70 include historical and projection experiments. The historical experiments include all-forcing (*historical*), greenhouse gas forcing only
71 (*historicalGHG*), natural forcing only (*historicalNat*), and other specific forcing (such as aerosols). The projection experiments consist
72 of four new representative concentration pathways (RCP)emission scenarios RCP2.6 through 8.5, representing anthropogenic radiative
73 forcing stabilizing at 2.6-8.5 W m⁻² by 2100 (Moss, 2010). In this study, we focus on the all-forcing *historical* and and *RCP4.5*
74 experiments, with limited exploration of the *historicalGHG* and *historicalNat* runs. The *historical* runs are forced by observed
75 atmospheric composition changes (reflecting both anthropogenic and natural sources). The temporal span of the *historical* experiment
76 covers 1851-2005, and thus is sometimes referred to as “20th century” simulations (Taylor et al, 2012). The *RCP4.5* scenario assumes
77 the anthropogenic forcing will essentially level off at 4.5 Wm⁻² around the mid-21st century and represents the intermediate range of
78 the four scenarios. *RCP4.5* runs cover 2005-2100 (some model groups extend it to 2300, see Thomson et al., 2001 for detail).

In this study, we analyze all available model ensemble members presently available in the *historical* and *RCP4.5* experiments, totaling 27 models and 163 members. The *historical* experiment has 25 models available with 100 members and the *RCP4.5* experiment encompasses 22 models with 63 members. Twenty out of 25 models in the *historical* experiment and 8 out of 22 models in the *RCP4.5* experiments have multiple ensemble members of 2 to 16 (Table 1). Monthly mean of daily maximum and minimum surface temperatures¹ from all models were mapped to a 1°x1° grid, the highest resolution of the models. The linear trends are computed based on a least squares regression. The horizontal resolution of the models ranges from 3.75° to 1.0°.

The observed daily temperatures used in this study were obtained from the Global Historical Climatology Network (GHCN) as compiled into monthly means and interpolated onto regular latitude/longitude grids by the Climate Research Unit (CRU). The data set includes monthly mean surface daily maximum and minimum temperatures on a 0.5°x0.5° latitude/longitude grid over land for the period 1901-2009 (New et. al., 2000; Mitchell and Jones, 2005; Vose et. al., 2005). Since data stations before the 1950's were somewhat sparse (New et al., 2000 for details), our analyses mainly focus on the temperature changes after the 1950s, although prior temperatures are also used to determine longer-term trends.

3. Observed cooling characteristics

¹ Most studies of GCM intercomparison use mean surface air temperature, masking the difference in maximum and minimum temperatures.

93 Since temperature variations are not monotonic but fluctuate, the trend values will depend on the evaluation periods. While
94 longer periods can give larger sample sizes, they may obscure underlying physical processes during different periods. For example,
95 the second half of the 20th century, an often-used period of recent studies (Wang et al., 2009), includes a period of global slight
96 cooling before 1975 and a strong warming period after that. To reduce the effect of arbitrarily choosing the lengths of periods, we
97 evaluated trends in three durations: 100 year (1901-2000), 50 year (1951-2000), and 25 year (1951-1975 and 1976-2000). The 100-
98 year duration represents the longest available data set and the 50-y period corresponds to the data-rich period. The separation of the 2nd
99 half of the century into two equal 25-y periods is not chosen for simplicity, but is based on following considerations: (1) The year
100 1976 is around the turning point of two climate epochs when the PDO shifted from a negative to a positive phase (Miller et al., 1994);
101 (2) The global temperature trend changed from a slight decrease to a strong increase around 1975 (Folland et al., 2002); and (3) The
102 year 1979 was the beginning of the satellite era when the incorporation of satellite data introduces some discontinuity in data sets
103 (Kalnay and Cai, 2003).

104 During the 20th century, the southeastern and central U.S. cooled up to 2°C (0.2 °C dec⁻¹), while most regions of the U.S.
105 warmed slightly (Fig. 1). On the half-century scale (1951-2000), the cooling along the southeast coast is more scattered, while summer
106 cooling expanded in the central U.S. On the quarter century scale (1976-2000), the summer WH became more concentrated in the
107 central U.S. with a cooling rate of over 0.6 °C dec⁻¹. It should be pointed out that this decrease of up to 1.5 °C for the 25-year period
108 (0.6°C dec⁻¹ for 2.5 decades) occurred when the global warming peaked. Almost all the global warming in the 20th century occurred in
109 this period (IPCC, 2007). Compared to summer when the WH and global temperature trends went in opposite directions, the winter

110 temperature in the whole eastern U.S. warmed by more than 3°C during the period, reflecting the sharp difference in forcing
111 mechanisms between summer and winter temperatures.

112 Figure 2 shows the daily maximum temperature (Tmax) trend in the 2nd half of the 20th century corresponding, respectively, to
113 the global cooling and warming periods. During 1951-75, when global mean temperature actually decreased slightly, the southeast
114 coastal region (SE) experienced sharp cooling of over 0.6°C dec⁻¹ along a wide swath in summer. During winter, the extensive cooling
115 spread over the central U.S. This seasonal cooling pattern is opposite of both the 2nd half of and the whole 20th century when the
116 summer cooling was situated in the central U.S., while winter cooling was along the SE. The Tmax trend pattern in 1976-2000 was
117 similar to that of the Tmean (mean of Tmax and Tmin in Fig. 1). Interestingly, from 1951-1975, when the PDO index was negative
118 (Nantau et al., 1997), the SE coastal region experienced sharp cooling, which seems to run against the established, negative correlation
119 between PDO and coastal temperature. During the last 25 years (1976-2000), which coincides with the peak global warming period,
120 the cooling shifted to the central section of the U.S. with cooling up to 0.6 °C dec⁻¹. Also during the 1976-2000 period, the summer
121 and winter trends are in opposite directions, with sharp warming in winter. An EOF analysis of the 50-year (1951-2000) period shows
122 two leading modes corresponding to the southeast(1st) and central (2nd) cooling, explaining more than 50% combined variance (Pan et
123 al., 2009).

124 One of global climate change signals is the widespread decline of daily temperature range (DTR). This is true especially in
125 winter starting from the 1950s and is the result of more rapid nocturnal warming than daytime warming (Karl et al. 1993; Dai et al
126 1999; Voss et al 2005). Global annual Tmin over land increased 0.20 °C dec⁻¹ while Tmax increased 0.14 °Cdec⁻¹) from 1950–2004,

127 resulting in a DTR decrease ($-0.07^{\circ}\text{Cdec}^{-1}$) (Voss et al., 2005). During the same period over North American land ($175\text{-}60^{\circ}\text{W}$, 15-
128 75°N), summer Tmax and Tmin increased 0.07 and $0.12^{\circ}\text{C dec}^{-1}$, respectively, resulting in -0.05°C in DTR change. A similar
129 decrease ($-0.06^{\circ}\text{Cdec}^{-1}$) occurred in winter. Over the central and southeast U.S. ($105\text{-}80^{\circ}\text{W}$, $30\text{-}45^{\circ}\text{N}$), summer Tmax actually
130 decreased sharply ($-0.13^{\circ}\text{Cdec}^{-1}$), while Tmin increased slightly ($0.05^{\circ}\text{Cdec}^{-1}$), yielding a DTR decrease of $0.18^{\circ}\text{Cdec}^{-1}$. Winter
131 DTR also decreased by $0.13^{\circ}\text{Cdec}^{-1}$.

132 Figure 3 shows the time series of surface temperature over central (CN) and southeast (SE) regions delineated in Fig. 2. The
133 U.S. temperature (both CN and SE) of the 20th century is characterized by the hot Dust Bowl period in 1930, followed by slight
134 cooling until the mid-1970s, and fast warming after that. This overall pattern is similar to the global mean, but with large fluctuations.
135 Separating temperatures into summer and winter as well as Tmax and Tmin shows that the U.S. temperatures deviate from the global
136 ones notably. In terms of summer daytime Tmax, the 1930s is still over 1°C warmer than other decades, including the globally
137 warmest 2010s. On the other hand, winter Tmin was greatest in the later 1990s and early 2000s. Globally, the temporal variations of
138 Tmax and Tmin during winter and summer follow similar patterns (dotted blue lines), while those of the U.S. (both CN and SE)
139 deviate from each other notably. Winter Tmin trends follow the global mean quite well (lower right panel, Fig.3). However, the Tmax
140 trends deviate from the global mean (top left). During 1985-1995, when global warming was quite fast, the U.S. Tmax decreased
141 sharply, indicative of the complex forcing in daytime during summer.

142 The time-latitudinal cross section along the red line in Fig. 2 shows the daytime warming in the 1930s Dust Bowl and cooling
143 after the 1960s, peaking in the 1990s during summer (top left panel, Fig. 4). The summer Tmin warming is mostly concentrated in the

144 1930s and 1990s at higher latitudes (top right panel). In winter, the Tmax and Tmin patterns are quite similar with warming in the
145 1930s and cooling in the 1960s-80s, as both are more likely controlled by large-scale dynamics as compared with summer when local
146 convection plays a role. The warming pattern, especially in the SE coastal region correlates well with the PDO index (bottom panel,
147 Fig. 4)

148

149 **4. CMIP5 model simulated 20th century cooling – *historical* experiment**

150 Here we present the model simulated temperature variations from 100 members of 25 models available in the *historical*
151 experiment. In our analysis, the ensemble mean of each model is first computed if the model has multiple members and then each
152 model contributes equally to the grand total mean of the 25 models. In other words, each model contributes to the ensemble mean with
153 equal weight regardless if the model has single or multiple members.

154 *a. Model ensemble means*

155 On the 100-year scale, the 25-model means seem to mimic the pattern of the SE cooling by showing slightly less warming than
156 surroundings. In winter, the region warms by $< 0.1^{\circ}\text{C dec}^{-1}$, which is much less than the warming in the rest of country (Fig. 5). The
157 presence of a WH is less evident in summer than winter. On the 50-y scale (1951-2000), the models showed a WH-like feature during
158 summer in the central U.S. Again the model did not show the absolute cooling as observed, but rather they showed a relative WH, i.e.,
159 lack of warming. The winter pattern shows a clear north-south (N-S) warming gradient as observed. On the quarter-century scale

160 (1975-2000), the models simulated more extensive warming in both summer and winter, although a swath of slightly less warming is
161 in the northern central U.S. in summer. Figure 6 shows Tmax in the globally cooling 1951-1975 period was simulated better than
162 globally warming period 1976-2000 period as compared with observations in Fig.2, meaning that the U.S. cooling is easier to be
163 captured when global trend is also cooling.

164 While there are different ways to classify models, horizontal resolution is a convenient one. The horizontal resolution varies by
165 about a factor of almost 4 among models. We chose six models (29 members) with the highest horizontal resolution (ACCESS,
166 CanCSM, CCSM4, CNRMS, CSIRO, and MRI-CGCM3). Figure 7 shows the 6-model means of Tmax and Tmin during the 2nd half of
167 the 20th century. These 6 models with the highest resolutions captured the WH and even over-predicted the WH somewhat. The WH
168 was most evident during summer in terms of Tmax with reasonable position and magnitude. Seasonality and Tmax/Tmin asymmetry
169 were also reproduced well.

170 Since the cooling in the SE is more persistent than CN over the whole 20th century (Fig. 1, top panels), we will focus our
171 attention on the SE cooling in this section. The time series of modeled SE temperatures show that models generally captured the
172 overall trend: slow rising before the 1940s, slight decreasing between the 1940s-1970s, and finally fast warming after the 1970s, but
173 the fluctuation (i.e., inter-annual variability) is smoother than the observations (Fig. 8). One interesting note is that the spread (grey
174 shaded area) simulated among different models in summer is narrower than winter. The best agreement among the models is Tmin in
175 summer where model spread brackets the observed trend all the time, partly because of smaller fluctuations in the observations. There
176 are times during the 1960s-1980s in winter when the observed temperature falls below the model spread when the SE temperature is

177 low. The summer model spread is narrower during the cooling period (1940s-1970s) and wider in warming periods before and after
178 that. The model spread widened after around the 1970s, especially in summer, when global mean temperature started to rise rapidly
179 after slight cooling in the 1940s.

180 *b. Inter-model variability*

181 The model ensemble mean represents all individual models that simulated diverse temperature patterns. As an example, Fig. 9
182 depicts the 25 individual simulations of Tmax during the 50-year period (1951-2000). About half of the models simulated a variant of
183 the WH pattern (less warming) in the general areas of the central-eastern U.S. A couple of models simulated an excessive warming
184 maximum around the WH region. As expected, within individual model families, the trend patterns are more similar. For example, the
185 HadGEM2 family consisting of three models/versions (-AO, -CC,-ES) generally simulated Mid-Atlantic warming and Pacific
186 Northwest cooling; the GISS-E2 family consisting of two models (-H, -R), simulated cooling in the western mountains and slightly
187 more warming along the East Coast. The only exception to the model family similarity is GFDL-ESM2 (-G, -M) whose two versions
188 simulated opposite trends in the southeastern coastal region.

189 To quantify the model skill in reproducing the WH phenomena, Fig. 10 shows the trends of 25 models in summer and winter
190 for Tmax and Tmin averaged over the SE WH region. On the century scale in summer (top left panel), the observed cooling only
191 occurred in summer during daytime (rightmost red bar denoted “O” on the X-axis). Six out of 25 models simulated negative trends
192 ranging from 0.005-0.04°C dec⁻¹ in summer. The remaining models simulated warming trends from 0.001-0.24 °C dec⁻¹. The all-

193 model mean is $+0.04^{\circ}\text{C dec}^{-1}$. All models except two simulated positive trends of T_{min}. The winter temperatures in the SE WH
194 region warmed during the century by $0.005\text{-}0.044^{\circ}\text{C dec}^{-1}$ (top right panel). Most models simulated positive trends, while five models
195 showed cooling trends.

196 On the 50-year scale (bottom panels), the observed cooling reached 0.4 (T_{min}) – 0.6 (T_{max}) $^{\circ}\text{C dec}^{-1}$ both in summer and
197 winter. The majority of models simulated warming on both T_{max} and T_{min} with an all-model mean of $+0.01^{\circ}\text{C dec}^{-1}$ (denoted “M” on
198 X-axis). Only three models produced negative trends of T_{max} with negligible magnitudes as compared with observations (bottom left).
199 In winter, 6 models simulated sizeable negative trends of temperatures. The observed DTR trend over the WH region was -0.25 to $-$
200 $0.3^{\circ}\text{C dec}^{-1}$ during 1951-2000 as indicated in Fig. 2, but was negligible or even positive in winter during the whole century. The
201 ensemble mean DTR trend was negligibly small ($<0.05^{\circ}\text{C dec}^{-1}$) compared to the observed trend of up to $0.3^{\circ}\text{C dec}^{-1}$.

202 One advantage provided by the CMIP5 experiments versus the CMIP3 is that the horizontal resolution of the atmospheric
203 components of the AOGCMs has improved. The roles of model spatial resolution have been examined in weather and climate models
204 both on regional and global scales. Its importance has been demonstrated by dynamically downscaling in climate simulations (Takle,
205 et al., 1999; Means, et al., 2009). Hack et al. (2006) found CAM3 simulations at T85 ($\approx 1.4^{\circ}$) had definite improvements in the larger-
206 scale dynamic circulations over those at T42. The GFDL AM2 simulation at higher resolutions was shown to more accurately depict
207 the East Asian frontal systems and the synoptic disturbances that propagate along the front (Lau and Ploshay, 2009). Shaffrey et al.
208 (2009) compared coupled simulations of the HiGEM ($0.83^{\circ}\times 1.25^{\circ}$) and HadGem ($1.25^{\circ}\times 1.875^{\circ}$) models developed at the UK Met.

209 Office and noted that the increased resolution gave better results in almost all aspects. Kinter et al. (2012) have shown the benefits of
210 higher resolution in global atmospheric model simulations of several features of climate variability.

211 All the above studies used a single model at various resolutions. Here we cannot evaluate the same model at different
212 resolutions, but rather we examine multiple models in a statistical sense since resolution difference among models is only one of many
213 other model differences as in Walsh et al. (2012). Also in the relatively flat central and southeastern U.S., to what extent model
214 resolution can improve model skills has been less studied. Fig. 11 shows the model bias in trend defined as the difference between
215 the modeled and observed trends in the SE region. Generally, the models of higher resolutions showed smaller biases (for the 50-year
216 period). The model biases tend to decrease with increasing resolution only over the medium range (110-180 grid points, roughly 2.5-
217 1.5°) for both temperatures in winter and summer. The skill improvement as resolution increases is most evident for summer during
218 the latter half of the 20th century, emphasizing the need for resolving local convection.

219 One feature of resolution is that the finest (resolution) models tend to have smaller bias spread among them. The four highest
220 resolution models on the right (Fig. 11) are always near their respective trend lines. On the other hand, the coarse models tend to have
221 larger spread in biases, although some have quite low biases. It also should be pointed out that those models of the same resolution
222 can give diverse biases because of different model formulations.

223 The inter-model variability is quantified in Fig. 12. All the model medians are positive for both periods in winter and summer.
224 Tmax is more dispersed than Tmin, especially on the 100-y scale in summer when the middle 50 percentile is about double of Tmin as

225 seen in Fig. 11. On the 100-year scale, the winter middle 50 percentile covers only $0.05\text{ }^{\circ}\text{C dec}^{-1}$ for T_{min} and $0.10\text{ }^{\circ}\text{C dec}^{-1}$ for T_{max}.
226 On the 50-year scale, summer warming is more than winter. Trends in most cases contain large positive outliers. The skews are
227 generally small with varying swings.

228 *c. Intra-model variability – internal dynamics*

229 This sub-section will compare results within individual models that have multiple member realizations. Since the model's
230 integration physics (and numerics) and external forcing remain the same, different initial conditions only represent internal variability
231 or model noise. In the CMIP5 experimental design, individual members are named drNiMpL where the triad (N, M, L) denotes ways
232 in which each initial condition is formed. N denotes different starting times from the same realistic time series; M, the initializing
233 method; and P, the way of physical perturbation. All models, but two, have only varying N, i.e., changing only in starting times. GISS-
234 E2-H and GISS-E2-Rruns have members with two ways of varying initial conditions (N and L). Figure 13 shows the T_{mean} trends
235 during 1951-2000 simulated by all 15 ensemble members in GISS-E2-H. The three panels in a given row (e.g., r1i1p1-p3 on the top
236 row) represent same initial time and initializing method, but with three different physical perturbations. Similarly, the five rows
237 represent different initial times. The 15 members vary significantly, but some patterns are still identifiable. The physical perturbation
238 method has larger impacts than the starting time². The middle column (L=2) tends to have sharp cooling comparable to the observed
239 WH extent, but located too far west as compared with the observations. On the other hand, in the right column strong warming

² The extent of the member spread may have been underestimated in CMIP5 experiments since the great majority of the models used varying start time only, not the perturbation method.

240 occurred over the observed cooling region. The intra-model variability of GISS-E2-H is quantified in Fig. 14 (bottom) along with the
241 other five models that have the most ensemble members. The percentile distributions showed more variability than the 25-model mean,
242 with less spread, partly due to their smaller sample size (6-16).

243 *d. External forcing*

244 Globally, it is very likely that the climatic warming observed over the past decades is attributable to human influences,
245 primarily to an increase in concentrations of well-mixed greenhouse gases (Meehl et al., 2004; IPCC, 2007). The anthropogenic signal
246 was detected in each of 14 regions of the globe except for one in central North America, although the results were more uncertain
247 when anthropogenic and natural signals were considered together (Taylor et al., 2012). In order to attribute observed climate change
248 to particular causes, it is essential to perform simulations of the historical period with only a subset of known forcing.

249 Like in CMIP3, CMIP5 designed the so-called attribution and detection experiments consisting of *historicalNat* and
250 *historicalGHG*, among others. The *historical* (all forcing) runs presented so far impose changing conditions (consistent with
251 observations), which include atmospheric composition (including CO₂), due to both anthropogenic and volcanic influences, solar
252 forcing, emissions or concentrations of short-lived species and natural and anthropogenic aerosols or their precursors, and land use
253 (Taylor et al., 2012). The natural forcing only experiment imposes natural variations (e.g., volcanoes and solar variability) evolving as
254 in the *historical* run. Correspondingly, the GHG forcing only experiment includes greenhouse gas forcing alone evolving as in the
255 *historical* run.

256 Whether the abnormal cooling in the central and southeastern U.S is caused by internal variability of the climate system or
257 forced by external forcing is a long-standing issue (Wang et al., 2009; Meehl et al., 2012). If the cooling is transient internal, the WH
258 regions would become warmer when the transient masking mechanism is gone in the future and the WH regions will “catch up” the
259 missed warming (Kunkel et al., 2006). If on the other hand, they are a response to the global warming forced by an external forcing, it
260 would likely continue to exist in the future. Several studies suggested the WHs are related to the PDO and AMO indices, an internal
261 variation of the atmosphere-ocean coupled system (Kunkel et al., 2006; Wang, et al., 2009; Meehl et al., 2012). Others suggested that
262 land surface processes and regional hydrological processes contribute to the cooling (Kalnay and Cai, 2003; Pan et al., 2004; Liang et.
263 al., 2006). Here we analyze the CMIP5 attribution experiments that include *historicalNat* and *historicalGHG* experiments.

264 Fewer models carried out these attribution experiments with less ensemble members compared with the *historical* and
265 *RCP4.5* runs. We evaluated 6 models with a single member: CCSM4, GFDL-ESM2M, GISS-E2-H, GISS-E2-R, MRI-CGCM3, and
266 NorESM1-M. Figure 15 shows that natural forcing only has a cooling effect in the central and northern U.S. in summer on the
267 century scale. The position matches quite well the observed CN WH. In the 2nd half of the 20th century, the northern tier of the U.S.
268 cooled considerably. Conversely, GHG forcing only would make the central U.S. warmer, particularly during the latter half of the
269 century in summer (Fig. 16). This suggests that GHGs would counteract the WH, rather than causing or enhancing it. The forcing
270 difference between the *historical* and *historicalNat* should reflect land use evolution, among other factors. Interestingly, the
271 difference showed a clear WH feature, especially in summer (Fig. 17). On the century scale, a large area of 0-0.05 °Cdec⁻¹ cooling
272 over the southeastern-central U.S. resembles the observed central WH very well. On the 50-year scale, the cooling extent retreated to

273 the southeast coast. In winter, the difference between the all-forcing and natural forcing experiments showed a general N-S warming
274 gradient, somewhat resembling the observed trend pattern in winter. The larger cooling difference between the two experiments in
275 the whole 20th century, rather than the latter half-century, perhaps reflects larger land use change during the earlier decades. The
276 larger impacts in summer, rather than winter, may be due to the larger roles that land surface processes play in the warm season due
277 to greater evapotranspiration etc. than in winter. If this is the case, the summer WH in the central and southeastern U.S. in the 20th
278 century is at least influenced by local/regional land surface processes, consistent with previous studies (Kalnay and Cai, 2003; Pan et
279 al., 2004; Liang et al., 2006)

280 Figure 18 compares trends under different scenarios over different periods and seasons. The GHG forcing only has strong
281 warming effects ($0.12\text{--}0.23\text{ }^{\circ}\text{C dec}^{-1}$) that may have partly compensated for cooling effects from the natural forcing in the all forcing
282 *historical* experiment. The *historical* experiment that incorporates both natural and anthropogenic forcing resulted in moderate
283 warming as seen in the *historical* experiment.

284

285 **5. Fate of warming hole in the 21st century as simulated in RCP4.5**

286 This section discusses the RCP4.5 simulations from 22 models with 63 ensemble members. One third (7) of the models had
287 multiple members ranging from 3-15 (Table 1). Following the same averaging procedure as in the *historical* experiment, Fig. 19
288 shows the ensemble mean of the projected Tmean over the first half of the 21st century (2006-2055). During summer, the northern

289 section of the U.S. warmed more than both lower and higher latitudes. The largest warming is located in the Great Lakes across to the
290 mountain region where T_{mean} would warm $0.4\text{--}0.5\text{ }^{\circ}\text{Cdec}^{-1}$. In winter, the strongest warming is over the northern U.S. all the way to
291 the north with a magnitude of more than $0.65^{\circ}\text{C dec}^{-1}$. This warming pattern both in winter and summer are very similar to the
292 simulated trend distributions for 1976-2000 (Figs. 5 and 6), the peak global warming period of the 20th century.

293 If we view model spread (maximum-minimum trends, contour lines in Fig. 19) as a measure of the uncertainty in the projection,
294 generally the areas of large uncertainty tend to coincide with large trends themselves. Perhaps the ratio of trend to inter-model
295 variance would be a better measure of model uncertainty. The highest ratios (or confidence) are over high latitudes in winter with
296 large trends and slightly large spread (right panel) and the lowest confidence is in summer over the U.S.-Mexico border, likely related
297 to the complex topography in the region.

298 The warming is faster during the first half of the 21st century and then slows down after about the 2050s (Fig. 20), consistent
299 with the leveling off of the atmospheric CO_2 concentration under the *RCP4.5* scenario. The diminishing warming and even cooling
300 during the latter periods of the 21st century, suggest the likely return of the WH, considering the models' underestimation of WHs in
301 the 20th century in the *historical* simulation.

302 The narrower spread of summer T_{mean} than winter is most likely due to the lesser variation in T_{min} as in the 20th century
303 simulation (Fig. 8). The model spread in *RCP4.5* is smaller than those in the *historical* runs, implying more agreements among the
304 models. For the whole 92 years (2006-2097), the SE T_{mean} increases $2.3\text{ }^{\circ}\text{C}$ with about 1.6°C in the first half.

305 During the first 50 years of the 20st century, the model ensemble mean showed 0.3-0.4°Cdec⁻¹ warming over SE region, ranging
306 from -0.01 (ACCESS) to 0.9 °C dec⁻¹ (Fig. 21). Tmax and Tmin warm at a similar rate, which differs from the 20th century simulations
307 where Tmax rose slower than Tmin. In fact, the summer Tmax rises faster than Tmin, a phenomenon rarely observed.

308

309 **6. Conclusions and Discussion**

310 A total of 163 ensemble members of long-term simulations from 27 AOGCMs available in the *historical* suite and *RCP4.5*
311 experiments are analyzed to examine the models' skill in reproducing the 20th century observed U.S. temperatures. The focus is on the
312 southeast and central regions where abnormal cooling occurred despite the fact that global warming accelerated during the 20th century.
313 To the author's knowledge, this study analyzed the largest number of AOGCM members to evaluate the collective skills of the climate
314 models. Unlike most climate studies with this kind of model evaluation, we evaluated maximum and minimum (Tmax and Tmin)
315 surface air temperatures separately rather than the mean of the two, although observational studies often separate the two temperatures.
316 With the separation, more detailed physical and dynamical processes can be revealed. For example, daytime Tmax is more associated
317 with land surface processes like evapotranspiration and land use types, while nocturnal Tmin should be more associated with large-
318 scale dynamics such as advection.

319 We evaluated model skills in three periods, 1901-2000, 1951-2000, and 1976-2000, corresponding to the whole 20th century,
320 the data rich period, and the peak global warming period, respectively. Over the 100-year period, the ensemble mean showed an area

321 of relatively less warming in the southeastern U.S., but over the 25-year period (1976-2000), models totally missed the central U.S.
322 cooling, even in a relative sense (i.e., relatively less or lack of warming). In addition, Tmin in winter was better simulated than Tmax
323 in summer when local forcing such as convection is strong. A subset of the six models with the finest resolution, reproduced the
324 warming hole in the central U.S. reasonably well both in the whole and the 2nd half of the 20th century. As model horizontal resolution
325 increases from 3.75° to 1°, the model bias in the southeastern U.S. decreases slightly, but fine resolution models tend to perform more
326 consistently among models compared to the coarse models that fluctuate among models in biases.

327 Data coverage is relatively sparse before 1950, especially outside the U.S. when computing the global means. So we focus on
328 the period 1951-2000 when most of the abnormal cooling occurred. For comparison, the projection is mostly evaluated in the first 50
329 years (2006-2055). For the second half the 20th century, the unbiased standard deviation (stdev) among the 25 models is around
330 0.12°C dec⁻¹ for both Tmax and Tmin as well summer and winter. We computed the intra-model variance of five models that have ≥6
331 members. The mean intra-model stdev varies from 0.06 °C dec⁻¹ in summer and 0.16 °C dec⁻¹ in winter. The large fluctuation in this
332 subset may partly be due to smaller sample size. The overall intra- and inter-model variances are comparable, around 0.12 °C dec⁻¹.
333 On the other hand, the bias (difference between modeled and observed trends) ranged from 0.45-0.7 °C dec⁻¹, nearly four times as
334 large as the model spread. This suggests, in a statistical sense, that model simulated trends are far off from the observed. The
335 observed trends are -0.7 °C dec⁻¹ for Tmax and 0.42 °C dec⁻¹ for Tmin, whereas most model simulated positive trends of 0.1-0.4
336 °Cdec⁻¹ (Fig. 9). By comparison, the projected trends during the next 50 years(2006-2055) is around 0.35 °C dec⁻¹, three times the
337 model spread, which assures us certain confidence in model projections.

338 Kunkel et al.(2006) analyzed 55 ensemble members' simulations of the 20th century and concluded that seven of 55 members
339 reproduced negative trends. In this study, we did not look into each individual member, but we found six out of 25 models (not
340 members) reproduced negative trends as observed. Although the delineations of WH areas and model groups differ in the two studies,
341 the percentages of negative trends simulated seem to point to a slight improvement of CMIP5 models over CMIP3 models.

342 The observed Tmax and Tmin showed different tracks. For example, summer Tmax decreased at 0.025 °C dec⁻¹ over the 20th
343 century while Tmin increased at a similar rate, resulting in a small trend in Tmean. Over the latter half of the 20th century, Tmax
344 decreased twice as fast as Tmin, but the model simulated trend differences between Tmax and Tmin are very small with both warming,
345 meaning that model's bias in trends more arises from misrepresenting Tmax trends.

346 The model spreads suddenly increased after around the 1970s, especially in summer, when global mean temperature started to
347 rise rapidly after slightly cooling since the 1940s. While it is difficult to pinpoint exact causes for the spread increase, a couple of
348 hypotheses can be offered here. The timing is close to the Great Shift of the Pacific SST oscillation around 1979 (Miller et al., 1994).
349 Models might capture the shift at different times and thus result in varying temperature phases since previous studies found that the
350 southeastern U.S. temperatures highly correlated to the PDO index (Wang, et al., 2009). Another possibility is that the Tmax trend
351 really started to depart from the Tmin trend and from global means during this period. Models may respond to this separation
352 differently, broadening the spread.

353 Whether the abnormal cooling is due to the atmospheric internal variability or external forcing is the focus of a number of
354 studies (Robinson et al., 2002; Wang et al., 2009; Meehl et al., 20012). The historical suite experiments in CMIP5 consisting of all
355 forcing (*historical*), GHG forcing only (*historicalGHG*), and natural forcing only (*historical* Nat) runs provide an opportunity to look
356 into this issue. The GHG forcing has a warming effect in the central U.S., implying that the warming hole (WH) is not due to the GHG
357 forcing. The difference between the all forcing and natural forcing only runs showed a well-defined cooling region resembling the WH
358 location, implying that local and regional surface processes may contribute to the WH.

359 Model results suggest that the fate of central and southeast WHs would likely depend on the relative magnitudes of GHG
360 forcing that contributes to warming and the natural forcing that contributes to cooling. If the GHG forcing is strong enough, the WHs
361 may be likely to disappear in the future.

362

363 **Acknowledgements**

364 We acknowledge the modeling groups, the Program for Climate Model Diagnosis and Intercomparison (PCMDI) and the
365 WCRP's Working Group on Coupled Modeling (WGCM) for their roles in making available the WCRP CMIP5 multi-model
366 dataset. Support of this dataset is provided by the Office of Science, U.S. Department of Energy. The U.S. authors acknowledges the
367 support of NOAA Climate Program Office "Modeling, Analysis, Predictions and Projections" (MAPP) Program as part of the CMIP5
368 Task Force.

369

370

371

372

373 **References**

- 374 Arora, V. K., and Coauthors, 2011: Carbon emission limits required to satisfy future representative concentration pathways of
375 greenhouse gases. *Geophys. Res. Lett.*, **38**, L05805, doi:10.1029/ 2010GL046270.
- 376 Boyle, J. and S. A. Klein, 2010: Impact of horizontal resolution on climate model forecasts of tropical precipitation and diabatic
377 heating for the TWP-ICE period. *J. Geophys. Res.*, **115**, D23113, doi:10.1029/2010JD014262.
- 378 Collins, M., S.F.B. Tett, and C. Cooper, 2001: The internal climate variability of HadCM3, a version of the Hadley Centre coupled
379 model without flux adjustments. *Clim. Dyn.* **17**, 61–81.
- 380 Donner, L. J., 2011: The dynamical core, physical parameterizations, and basic simulation characteristics of the atmospheric
381 component AM3 of the GFDL Global Coupled Model CM3. *J. Clim.*, **24**, DOI:10.1175/2011JCLI3955.1.
- 382 Dunne, J.P., 2012: GFDL’s ESM2 global coupled climate-carbon Earth System Models Part I: Physical formulation and baseline
383 simulation characteristics, *J. Clim.*, DOI: 10.1175/JCLI-D-11-00560.1
- 384 Folland, C. K., et al., 2002: Observed climate variability and change, in *Climate Change 2001: The Scientific Basis—Contribution of*
385 Working Group I to the Third Assessment Report of the Intergovernmental Panel on Climate Change, edited by J. T. Houghton
386 et al., pp. 99 – 181, Cambridge Univ. Press, New York.
- 387 Gent, P. R., et.al. 2011: The Community Climate System Model version 4. *J. Clim.*, doi: 10.1175/2011JCLI4083.1
- 388 Hack, J., J. M. Caron, G. Danabasoglu, K. W. Oleson, C. Bitz, and J. Truesdale, 2006: CCSM-CAM3 climate simulation sensitivity to
389 changes in horizontal resolution, *J. Clim.*, **19**, 2267–2289.
- 390 Holland, M. M., and C.M. Bitz, 2003: Polar amplification of climate change in coupled models, *Clim. Dyn.*, **21**, 221–232.

391 Hourdin et al, The LMDZ4 general circulation model : climate performance and sensitivity to parametrized physics with emphasis on
 392 tropical convection, *Clim. Dyn.*, **27** : 787-813.

393 IPCC, 2007: *Climate Change 2007: The Physical Science Basis. Contribution of Working Group I to the Fourth Assessment Report of*
 394 *the Intergovernmental Panel on Climate Change* [Solomon, S., D. Qin, M. Manning, Z. Chen, M. Marquis, K.B. Averyt,
 395 M.Tignor and H.L. Miller (eds.)]. Cambridge University Press, Cambridge, United Kingdom and New York, NY, USA.

396 Jones, C.D., et al. 2011: The HadGEM2-ES implementation of CMIP5 centennial simulations, *Geosci. Model Dev.*, **4**, 543–570,
 397 doi:10.5194/gmd-4-543-2011.

398 Kalnay, E. and M. Cai, 2003: Impact of urbanization and land-use change on climate. *Nature*, **423**, 528-531.

399 Karl, T.R. et al., 1993. A new perspective on recent global warming: asymmetric trends of dally maximum and minimum temperature.
 400 *Bull. Am. Meteorol. Soc.*, **74**, 1007-1023.

401 Kinter III, J. L. et al., 2012: Revolutionizing climate modeling - Project Athena: A multi-institutional, international collaboration. *Bull.*
 402 *Amer. Meteor. Soc.* (in press).

403 Kumar. S., J. L. Kinter III, P. A. Dirmeyer, Z. Pan, and J. Adams, 2012: Multi-decadal climate variability and the “warming hole” in
 404 North America - results from CMIP5 climate simulations. *J. Climate* (submitted).

405 Kunkel, K.E., X.-Z. Liang, J. Zhu, and Y. Lin, 2006: Can CGCMs simulate the twentieth century "warming hole" in the central United
 406 States. *J. Climate*, **19**: 4137-153.

407 Lau, N.C., and J. J. Ploshay, 2009: Simulation of synoptic- and subsynopticscale phenomena associated with the East Asian summer
 408 monsoon using a high-resolution GCM, *Mon. Weather Rev.*, **137**, 137–160.

409 Liang, X.-Z., J. Pan, J. Zhu, K. E. Kunkel, J. X. L.Wang, and A. Dai, 2006: Regional climate model downscaling of the US. summer
 410 climate and future change. *J. Geophys. Res.*, **111**, D10108, doi:10.1029/2005JD006685.

411 Liu, X.D. and B.D. Chen, 2000: Climatic warming in the Tibetan Plateau during recent decades, *Intl. J. of Clim.*, **20**, 1729-1742.

412 Maloney, E. et al., 2012: North American Climate in CMIP5 Experiments: Part III: Assessment of 21st Century Projections *J. Climate*
413 (submitted).

414 Mantua, N.J., S.R. Hare, Y. Zhang, J.M. Wallace, and R.C. Francis, 1997: A Pacific decadal climate oscillation with impacts on
415 salmon. *Bull. Amer. Meteor. Soc.*, **78**, 1069-1079.

416 Mearns, L., and Coauthors, 2009: A Regional Climate Change Assessment Program for North America. *Eos Trans. AGU*, **90**, 311-312.

417 Meehl, G. A., J. M. Arblaster, and G. Branstator, 2012: Mechanisms contributing to the warming hole and the consequent U.S. east-
418 west differential of heat extremes. *J. Climate* (in press).

419 Meehl, G. A., W. M. Washington, C. M. Ammann, J. M. Arblaster, T. M. L. Wigley, and C. Tebaldi, 2004: Combinations of natural
420 and anthropogenic forcings in 20th century climate, *J. Clim.*, **17**, 3721– 3727.

421 Miller, A., D. Cayan, T. Barnett, N. Graham, and J. Oberhuber, 1994: The 1976–77 climate shift of the Pacific Ocean. *Oceanography*, **7**,
422 21–26.

423 Moss, R. H., 2010: The next generation of scenarios for climate change research and assessment. *Nature*, **463**, 747–
424 756, doi:10.1038/nature08823, 2010.

425 New, M. G., M. Hulme, and P. D. Jones, 2000: Representing 20th century space-time climate variability. II: Development of 1901-
426 1996 monthly terrestrial climate fields, *J. Climate*, **13**, 2217-2238.

427 Pan, Z., R.W. Arritt, E.S. Takle, W.J. Gutowski, Jr., C.J. Anderson, and M. Segal, 2004: Altered hydrologic feedback in a warming
428 climate introduces a “warming hole”. *Geophys. Res. Lett.*, 31, L17109, doi:10.1029/2004GL02528.

429 Pan, Z., M. Segal, X.-Z. Li, and B. Zib, 2009: Global climate change impact on the Midwestern U.S - a summer cooling trend. IN
430 “*Regional Climate Variability, Predictability, and Change in Midwestern USA*, edit by S. Pryor, Indiana University Press.

431 Portmann, R. W., S. Solomon, and G. C. Hegel, 2009: Spatial and seasonal patterns in climate change, temperatures, and precipitation
432 across the United States. *Proc. Nat. Acad. Sci.*, USA, 106: 7324-7329.

433 Raddatz et al., 2007. Will the tropical land biosphere dominate the climate-carbon cycle feedback during the twenty first century?
434 *Clim. Dyn.*, **29**, 565-574, doi 10.1007/s00382-007-0247-8

435 Robinson, W. A., R. Reudy, and J. E. Hansen, 2002: General circulation model simulations of recent cooling in the east-central United
436 States. *J. Geophys. Res.*, 10.1029/2001JD001577.

437 Rotstayn, L., Collier, M., Dix, M., Feng, Y., Gordon, H., O Farrell, S., Smith, I. and Syktus, J. 2010: Improved simulation of
438 Australian climate and ENSO-related climate variability in a GCM with an interactive aerosol treatment. *J. Clim.*, **30**, 1067-
439 1088, DOI 10.1002/joc.1952 b.

440 Schmidt, G.A., 2006: Present day atmospheric simulations using GISS ModelE: Comparison to in-situ, satellite and reanalysis data. *J.*
441 *Climate*, **19**, 153-192, doi:10.1175/JCLI3612.1.

442 Shaffrey, L. C., et al., 2009, U.K. HiGEM: The new U.K. high-resolution global environment model-model description and basic
443 evaluation, *J. Clim.*, **22**, 1861–1896.

444 Sheffield, J. et al., 2012: North American climate in CMIP5 Experiments: Part I: Evaluation of 20th century continental and regional
445 climatology. *J. Climate* (submitted).

446 Sheffield, J. et al., 2012: North American climate in CMIP5 Experiments: Part II: Evaluation of 20th century intra-seasonal to decadal
 447 variability. *J. Climate* (submitted).

448

449

450 Takle, E., W. Gutowski, R. Arritt, Z. Pan, and co-authors, 1999: Project to Intercompare Regional Climate Simulations (PIRCS):
 451 description and initial results. *J. Geophys. Res.*, **104**, 19,443-19,462.

452 Taylor, K. E., R. J. Stouffer, and G. A. Meehl, 2012: An overview of CMIP5 and the experiment design. *Bull. Amer. Meteor. Soc.*, **93**,
 453 485–498.

454 Tett S.F.B.; *et al.*, 2002: Estimation of natural and anthropogenic contributions to twentieth century temperature change. *J. Geophys.*
 455 *Res.* **10**, DOI:10.1029/2000JD000028.

456 Thomson, A. et al., 2011: *RCP4.5: a pathway for stabilization of radiative forcing by 2100. Climatic Change*, 109, 77-94. DOI:
 457 10.1007/s10584-011-0151-4.

458 Vose, R. S., D. R. Easterling, and B. Gleason, 2005: Maximum and minimum temperature trends for the globe: An update through
 459 2004, *Geophys. Res. Lett.*, **32**, L23822, doi:10.1029/2005GL024379.

460 Voldoire, A., et al., 2012: The CNRM-CM5.1 global climate model: description and basic evaluation, *Clim. Dyn.*, DOI
 461 10.1007/s00382-011-1259-y.

462 Volodin, E.M., N. A. Dianskii, and A. V. Gusev, 2010: Simulating present-day climate with the INMCM4.0 coupled model of the
 463 atmospheric and oceanic general circulations. *Atmos. and Ocen. Phys.* **46**, 414–431

- 464 Walsh, K., S. Lavender, E. Scoccimarro, and H. Murakami, 2012: Resolution dependence of tropical cyclone formation in CMIP3 and
465 finer resolution models. *Clim. Dyn.*, DOI:10.1007/s00382-012-1298.
- 466 Wang, H., S. Schubert, M. Suarez, J. Chen, M. Hoerling, A. Kumar, P. Pegion, 2009: Attribution of the seasonality and regionality in
467 climate trends over the United States during 1950-2000. *J. Climate*, **22**, 2571-2590.
- 468 Watanabe, M., and Coauthors, 2010: Improved climate simulation by MIROC5: Mean states, variability, and climate sensitivity. *J.*
469 *Clim.*, **23**, 6312–6335.
- 470 Wu, T., R. Yu, F. Zhang, et al., 2010: The Beijing Climate Center for Atmospheric General Circulation Model (BCC-AGCM2.0.1):
471 Description and its performance for the present-day climate. *Clim. Dyn.*, **34**, 123-147.
- 472 Yukimoto et al., 2011: Meteorological Research Institute-Earth System Model Version 1 (MRI-ESM1) - Model description, Technical
473 Report of the Meteorological Research Institute, 64, 83pp.) (Available online:
474 http://www.mri-jma.go.jp/Publish/Technical/DATA/VOL_64/tec_rep_mri_64.pdf)
- 475 Zhou, T. J., and Coauthors, 2005: The climate system model FGOALS s using LASG/IAP spectral AGCM SAMIL as its atmospheric
476 component. *Acta Meteorologica Sinica*, 63, 702-715. (in Chinese)

481 **Table and Figure captions**

482 Table 1. Characteristics of models participated in *historical* and *RCP4.5* experiments. Listed are 25 models in *historical* experiments
483 and 23 in *RCP4.5* experiment. The first number in the first column before the slash is model ID in *historical* and the second is model
484 ID in *RCP4.5* experiment.

485 Fig. 1. Linear trends of observed mean surface air temperature on 100-year, 50-year, and 25-year scales during periods of the 20th
486 century, showing southeastern and central U.S. cooling, while the globe experienced unprecedented warming.

487 Fig. 2. Linear trends of observed maximum surface air temperature during the 2nd half of the 20th century when the cooling was most
488 evident. The red rectangles on the top panels represent the southeast (SR, left) and central (CN, right) warming holes (WHs),
489 respectively. The red line on the bottom left panel represents the meridional cross-section passing through the two WHs. The SE WH
490 covers 105-80°W and 30-40°N while the CNWH covers 110-85°W and 35-45°N. The cross section line runs from 30-50°N along the
491 95°W meridian.

492 Fig. 3. Time series of surface Tmax/Tmin in the WH regions as compared with the global land means, contrasting distinctions
493 between Tmax vs. Tmin, winter vs. summer, and central vs. southeast coastal regions. The central and coastal regions are identified in
494 Fig. 2. The global means are over land only. Values plotted are the anomalies from the 109 y (1901-2009) mean. The cosine latitude is
495 used for weighted averaging in space.

496 Fig. 4. Upper: Latitude-time cross section of linear trends of temperature anomaly along 95°W as defined in Fig. 2. Lower: time series
 497 of PDO index based on the leading EOF amplitude.

498 Fig. 5. Twenty five model mean of linear trends of mean surface air temperature on 100-y, 50-y, 25-y time scales of the 20th century.
 499 Each model equally contributes to the ensemble mean regardless of whether they have multiple or single ensembler members.

500 Fig. 6. Twenty-five model mean of linear trends of maximum surface air temperature during the 1951-1975 and 1976-2000 periods,
 501 corresponding to peaking cooling periods over the southeastern WH and central WH, respectively.

502 Fig. 7. Linear trends of mean surface air temperature during 1951-2000 periods computed only from six models of the highest
 503 resolutions (ACCESS, CanCSM, CCSM4, CNRMS, CSORO, and MRI-CGCM3), totaling 28 members.

504 Fig. 8. Time series of SE WH surface temperature anomaly during summer (top) and winter (bottom) simulated by 25 models in the
 505 historical experiment. The five curves of individual models are those with the largest numbers of ensemble members. The shaded
 506 areas bracket maximum and minimum trends among the 25 models. Values plotted are the anomalies from the 109 year (1901-2009)
 507 mean. The cosine of latitude is used for weighted averaging in space. A 7-year running mean in time was applied.

508 Fig. 9. Linear trends of Tmax simulated by the 25 models during 1951-2000. For those models with multiple members, the panel is
 509 the average of all members of the model.

510 Fig. 10. Trends of Tmax and Tmin over the southeast WH in summer and winter during 1901-2000 and 1951-2000 periods. The model
 511 IDs are listed in Table 1. The right most two dual-bars represent all model mean (M) and observation (O), respectively.

512 Fig. 11. Scatter plot of model biases (modeled – observed trends) versus model horizontal resolution expressed in grid points for 1901-
513 2000 (01-00) and 1951-2000 (51-00).

514 Fig. 12. Statistics of 25-model simulated southeast WH temperature trends in summer and winter during the whole and half of the 20th
515 century. 100yS(W): 1901-2000 summer (winter); 50yS(W): 1951-2000 summer(winter).

516 Fig. 13. Linear trends of Tmax simulated by the 15 individual members of GISS-E2-H model during 1951-2000. The triad of integers
517 in ensemble member (i.e., panel) named NiMpL(N, M ,L) denotes initial time, initiation method, and perturbation physics,
518 respectively.

519 Fig. 14. Same as Fig. 12 but, for Tmax of individual models that have more than 8 ensemble members.

520 Fig. 15. Six-model ensemble mean of linear trends of Tmean simulated in the *historicalNat* experiment in summer (left) and winter
521 (right) during 1901-2000 (top) and 1951-2000 (bottom).

522 Fig. 16. Same as Fig. 15, but for *historicalGHG*.

523 Fig. 17. Same as Fig. 15, but for the difference between all forcing (*historical*) and natural forcing only (*historicalNat*) experiments.

524 Figure 18. Comparison of Tmean trends in the southeast WH under different scenarios for different durations in summer and winter.

525 Fig. 19. Linear trend of Tmean during 2006-2055 averaged among 22 models with 63 members in the *RCP4.5* experiment. The
526 contours are the inter-model spread.

527 Fig. 20. Time series of Tmean in the southeast WH simulated by 22 models in the *RCP4.5* experiment. The five curves of individual
528 models are those with the largest numbers of ensemble members. The shaded areas bracket maximum and minimum values among the
529 22 models. The values plotted are anomalies from the 92-y mean (2006-2097) and the WH average is weighted using cosine of the
530 latitude as the weight. A 7-year running mean in time was applied.

531 Fig. 21. Twenty-two model projected southeast WH temperature trend during 2006-2055. Model IDs are given in Table 1. The
532 rightmost bars are the model mean.

533

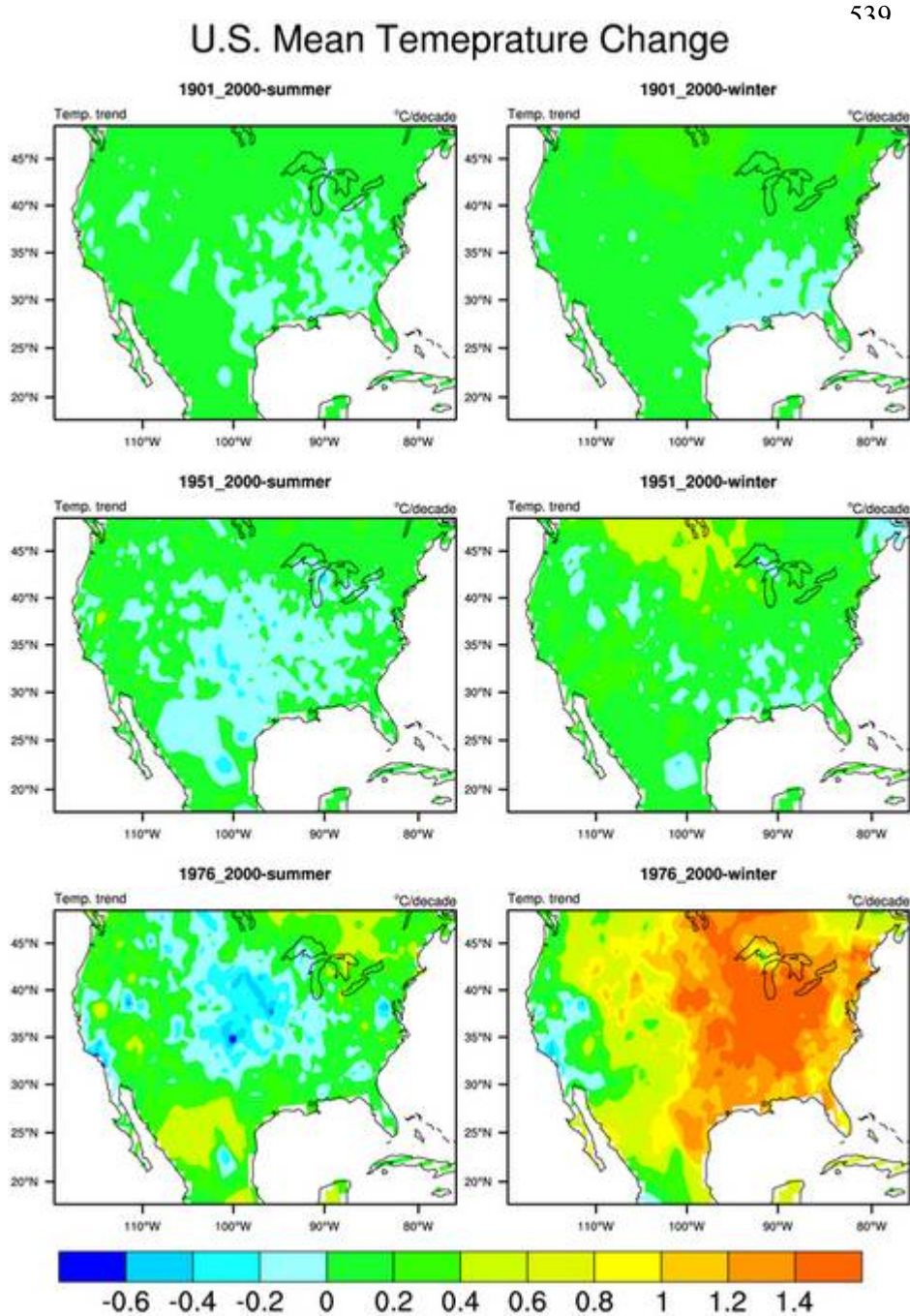
534 Table 1. Characteristics of models participated in *historical* and *RCP4.5* experiments. Listed are 25 models in *historical* experiments
535 and 23 in *RCP4.5* experiment. The first number in the first column before the slash is model ID in *historical* and the second is model
536 ID in *RCP4.5* experiment.

Model ID (hist/rcp4.5)	Model symbol	Model Center	Atm. Res. (lon. x lat.)	No of atm. layers	Members (<i>Historical</i>)	Members(<i>RCP4.5</i>)	Reference
1/1	ACCESS1-0	CSIRO and BOM (Bureau of Meteorology, Australia	1.875 x 1.25	38	1	1	http://wiki.csiro.au/confluence/display/ACCESS
2/2	BCC-CSM1.1	Beijing Climate Center, China Meteorological Administration, China	2.8 x 2.8	17	3	1	Wu et al.,2011
-/3	Bnu-esm	Beijing Normal University, Beijing, China	2.8x2.8	22	-	1	Ji Duoying (duoyingji@bnu.edu.cn)
3/4	CanESM2	Canadian Center for Climate Modeling and Analysis, Canada	2.8 x 2.8	22	5	5	Arora et al., 2011, Gent, et. al., 1998
4/5	CCSM4	National Center for Atmospheric Research, USA	1.25 x 1.0	17	6	5	Gent et al., 2011
5/6	CNRM-CM5.1	National Centre for Meteorological Research, France	1.4 x 1.4	17	8	1	Voldoire et al., 2011

6/7	CSIRO-MK3.6	CSIRO and Climate Change Centre of Excellence, Australia	1.8 x 1.8	18	10	10	Rotstayn et al., 2010
7/-	FGOALS-S2.0	LASG, Institute of Atmospheric Physics, Chinese Academy of Sciences	2.8 x 1.6	17	3	-	Zhou et al., 2005
8/-	GFDL-CM3	NOAA Geophysical Fluid Dynamics Laboratory, USA	2.5 x 2.0	23	4	-	Donner et al., 2011
9/-	GFDL-ESM2G	As in GFDL-CM3	2.5x2.0	23	1	-	Dunne, et al., 2012
10/8	GFDL-ESM2M	As in GFDL-CM3	2.5x2.0	23	1	1	As in GFDL-CM3
11/-	GISS-E2-H	As in GFDL-CM3	2.5 x 2.0	17	15	-	Schmidt et al., 2006
12/-9	GISS-E2-R	As in GISS-E2-H	2.5 x 2.0	17	16	15	Schmidt et al., 2006
13/-	HADCM3	Met Office Hadley Centre, UK	2.5x3.75	23	1	-	Collins, et al., 2001
14/10	HadGEM2-AO	As in HADCM3	1.8 x 1.25	23	1	1	Jones et al., 2011
15/11	HadGEM2-AO	As in HADCM3	1.8 x 1.25	23	1	1	As in HADCM3

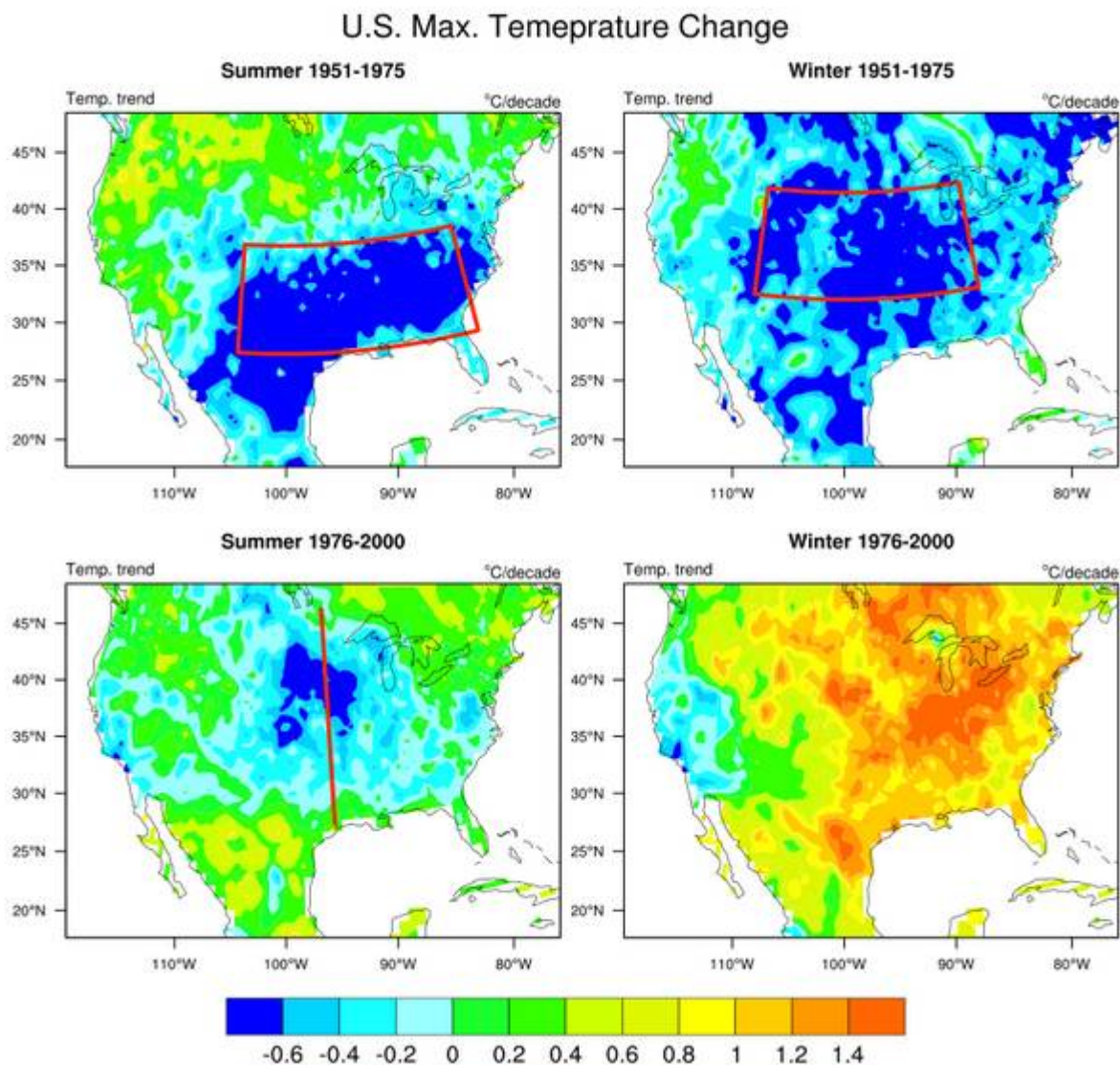
16/12	HadGEM 2-ES	As in HADCM3	1.8 x 1.25	23	1	4	As in HADCM3
-/13	inmcm4		1.5 x 2.0	17	-	1	Volodin, et al., 2010
17/14	IPSL-CM5A-LR	Institut Pierre Simon Laplace, France	3.75 x 1.8	17	5	4	Hourdin et al., (2011)
18/15	IPSL-CM5A-MR	As in IPSL-CM5A-LR	3.75 x 1.8	17	2	1	As in IPSL-CM5A-LR
-/16	IPSL-CM5B-LR	As in IPSL-CM5A-LR	3.75 x 1.8	17	-	1	As in IPSL-CM5A-LR
21/17	MIROC5	Atmos and Ocean Res. Inst., Agency for Marine-Earth Sci & Tech, Japan	1.4 x 1.4	17	4	3	Watanabe et al., 2010
19/18	MIROC-ESM	As in MIROC5	2.8x2.8	17	1	1	As in MIROC5
20/19	MIROC-ESM-CHEM	As in MIROC5	1.4 x 1.4	17	1	1	As in MIROC5
22/20	MPI-ESM-LR	Max Planck Institute for Meteorology, Germany	1.9 x 1.9	25	3	3	Raddatz et al., 2007
23/-	MPI-ESM-P	As in MPI-ESM-LR	1.9 x 1.9	25	2	-	As in MPI-ESM-LR

24/21	MRI- CGCM3	Meteorological Research Institute, Japan	1.1 x 1.1	23	4	1	Yukimoto et al., ⁵³⁷ 2011
25/22	NorESM1 -M	Norwegian Climate Center, Norway	2.5 x 1.9	17	1	1	N/A



543

544 Fig. 1. Linear trends of observed mean surface air temperature on 100-year, 50-year, and 25-year
 545 scales during periods of the 20th century, showing southeastern and central U.S. cooling, while
 546 the globe experienced unprecedented warming.



548

549 Figure 2. Linear trends of observed maximum surface air temperature during the 2nd half of the
 550 20th century when the cooling was most evident. The red rectangles on the top panels represent
 551 the southeast (SR, left) and central (CN, right) warming holes (WHs), respectively. The red line
 552 on the bottom left panel represents the meridional cross-section passing through the two WHs.
 553 The SE WH covers 105-80°W and 30-40°N while the CN WH covers 110-85°W and 35-45°N.
 554 The cross section line runs from 30-50°N along the 95°W meridian.

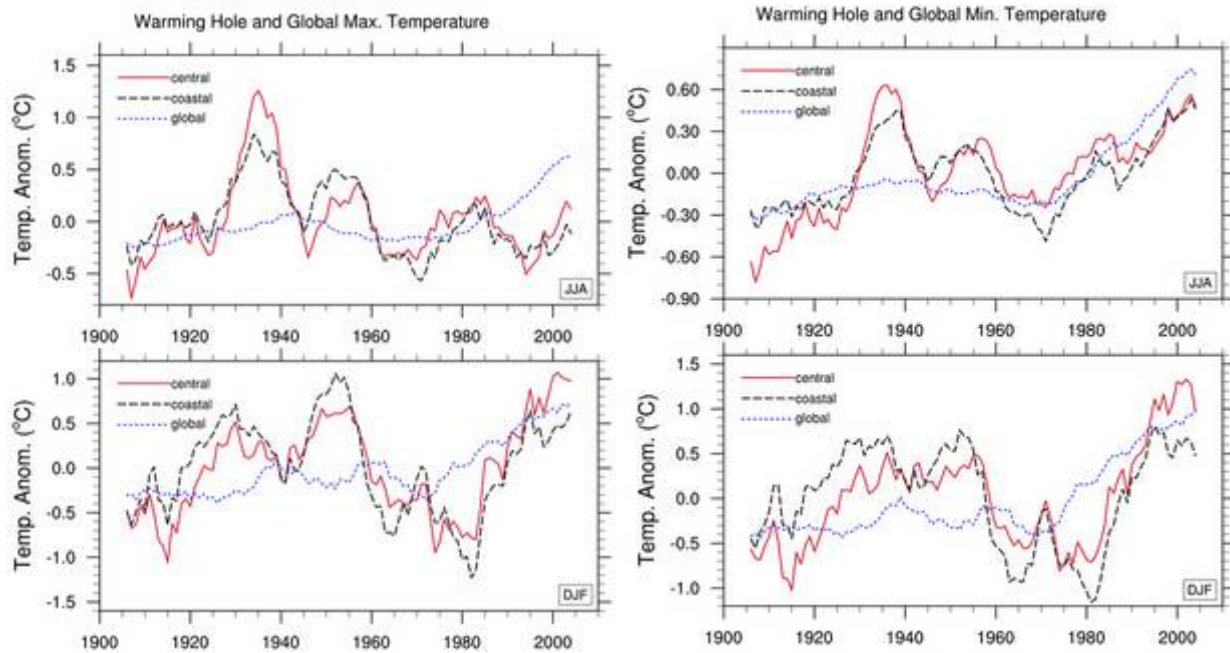


Fig. 3. Time series of surface Tmax/Tmin in the WH regions as compared with the global land means, contrasting distinctions between Tmax vs. Tmin, winter vs. summer, and central vs. southeast coastal regions. The central and coastal regions are identified in Fig. 2. The global means are over land only. Values plotted are the anomalies from the 109 y (1901-2009) mean. The cosine latitude is used for weighted averaging in space.

555

556

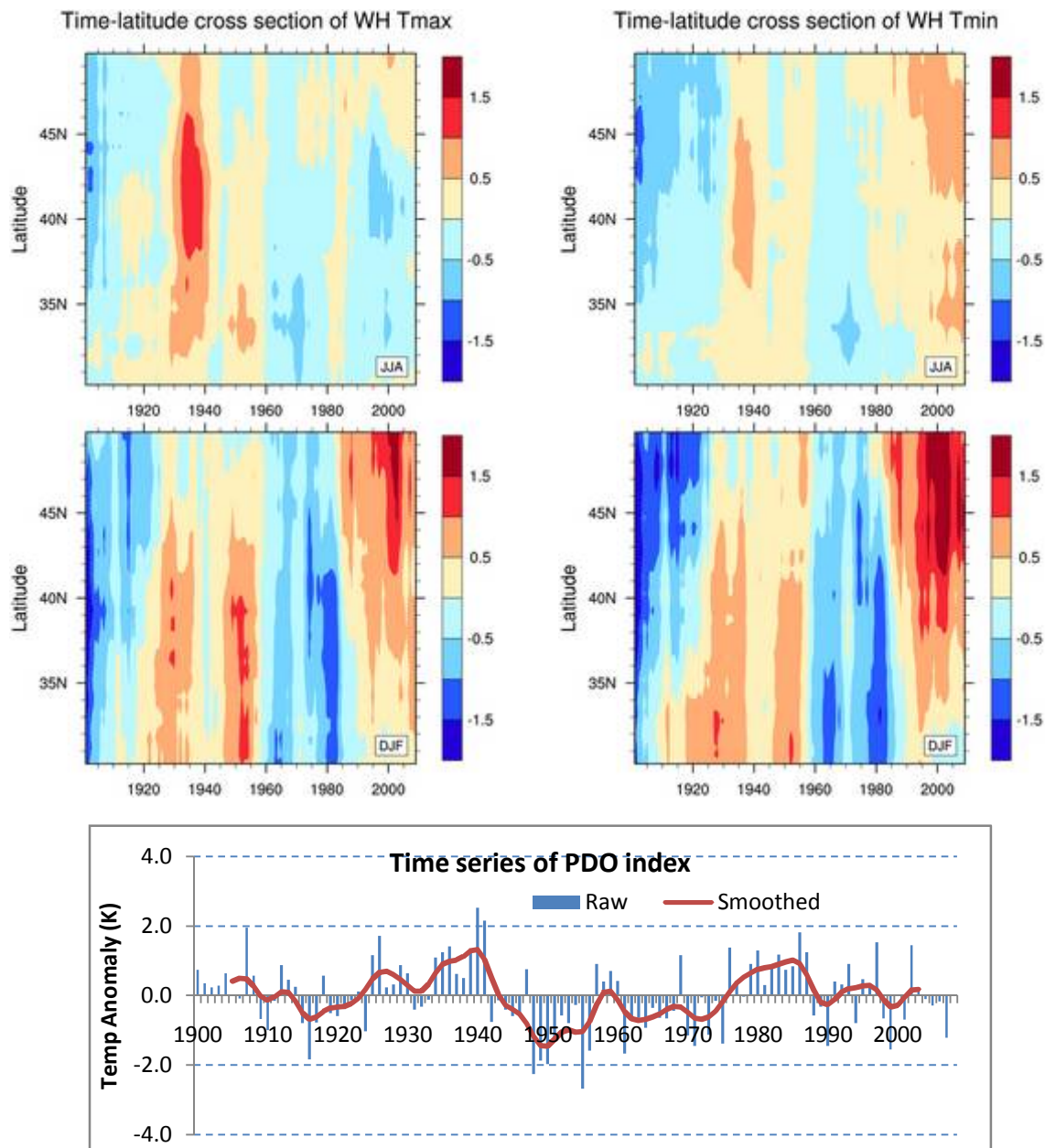


Fig. 4. Upper: Latitude-time cross section of linear trends of temperature anomaly along 95°W as defined in Fig. 2. Lower: time series of PDO index based on the leading EOF amplitude.

557

558

Trend of Mean Surface Temperature - 25 model ensemble mean

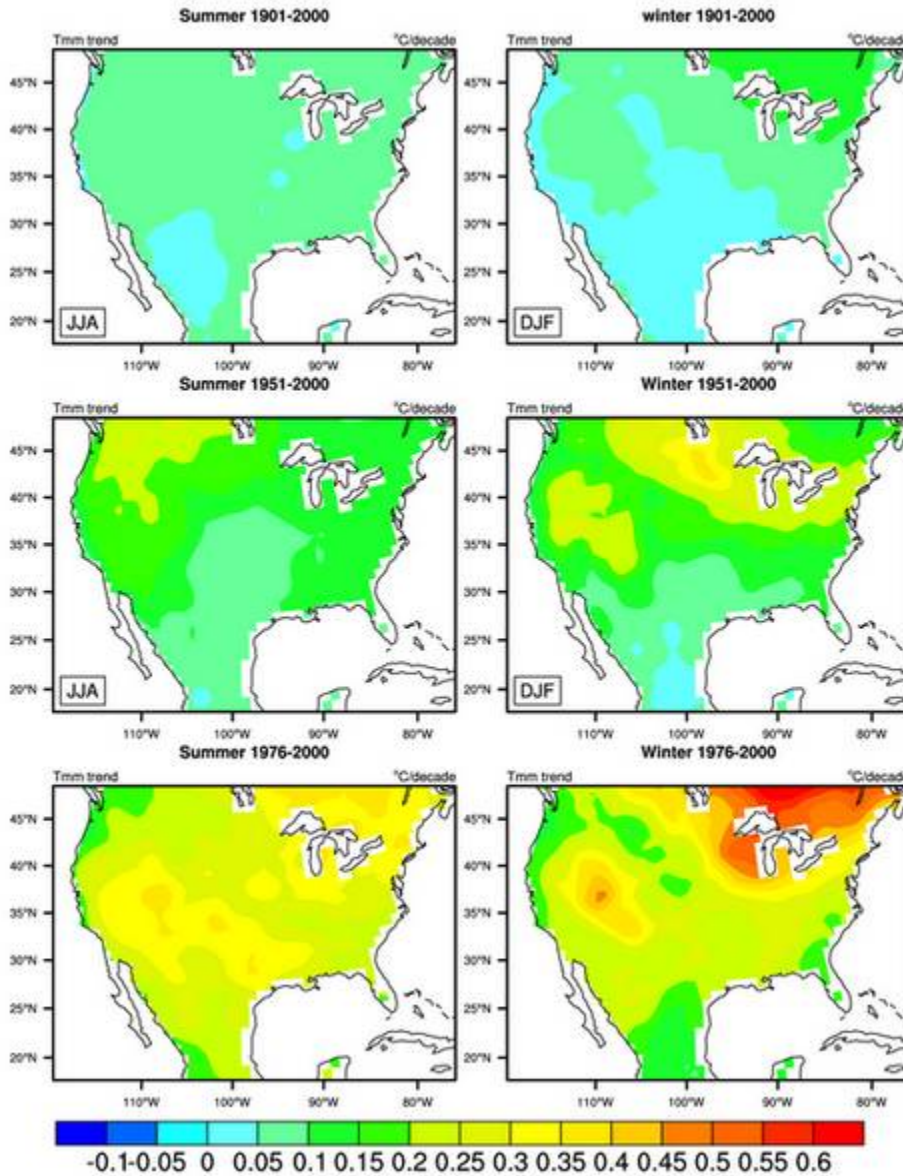


Fig. 5. Twenty five model mean of linear trends of mean surface air temperature on 100-year, 50-year, 25-year time scales of the 20th century. Each model equally contributes to the ensemble mean regardless whether they have multiple or single ensemble members.

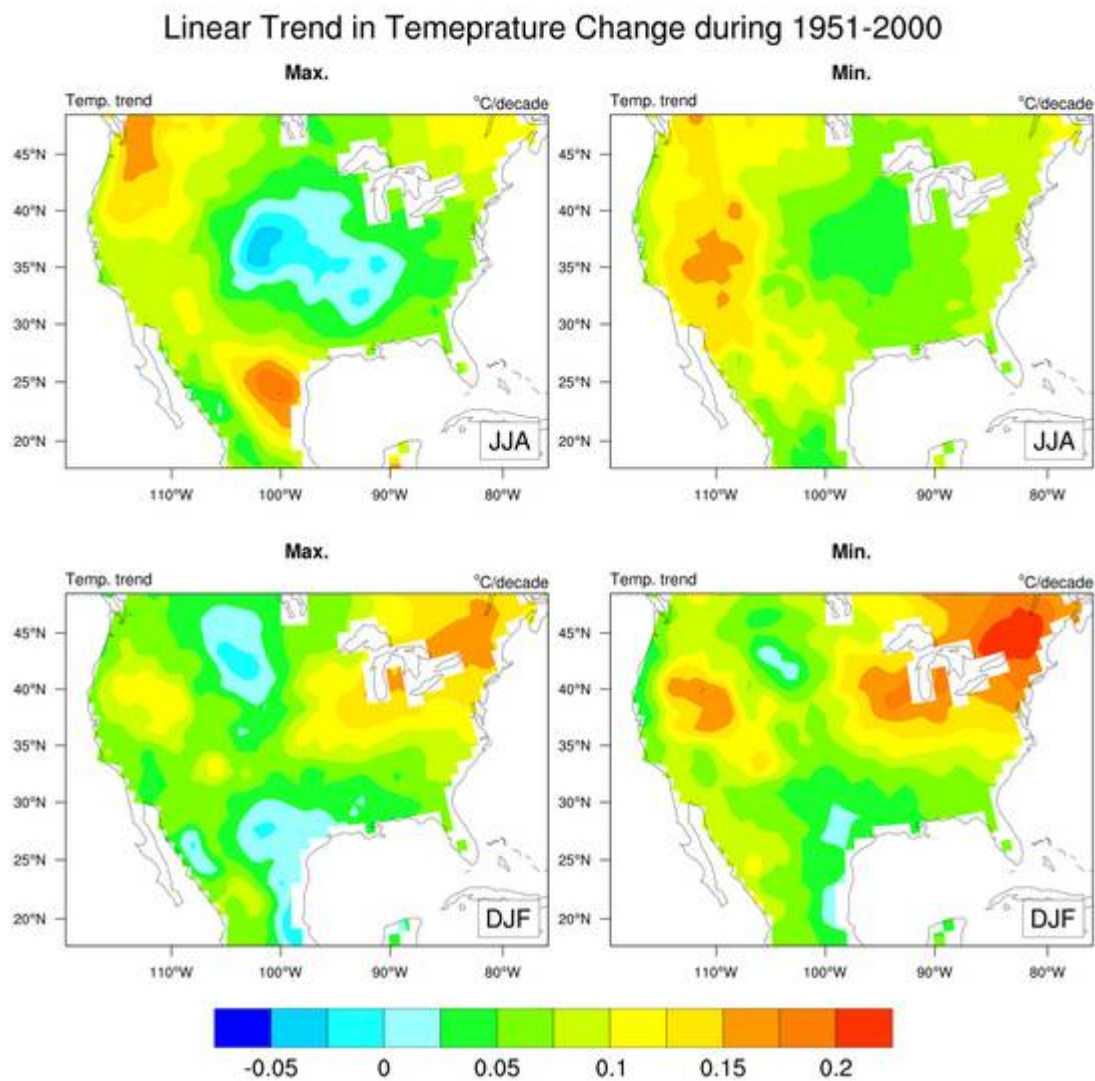


Fig. 7. Linear trends of mean surface air temperature during 1951-2000 periods computed only from six models of highest resolutions (ACCESS, CanCSM, CCSM4, CNRMS, CSORO, and MRI-CGCM3), totaling 28 members.

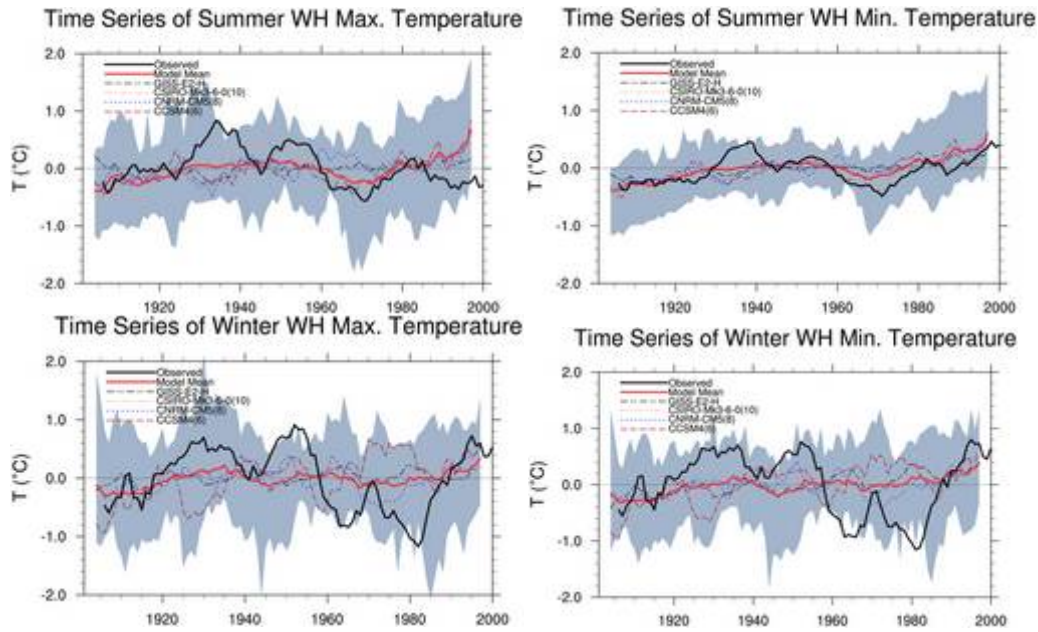


Fig. 8. Time series of SE WH surface temperature anomaly during summer (top) and winter (bottom) simulated by 25 models in the historical experiment. The five curves of individual models are those with the largest numbers of ensemble members. The shaded areas bracket maximum and minimum trends among the 25 models. Values plotted are the anomalies from the 109 year (1901-2009) mean. The cosine of latitude is used for weighted averaging in space. A 7-year running mean in time was applied.

592 ftp://ftp.eas.slu.edu/pub/panz/proj_26new.png Fig. 9. Linear trends of Tmax simulated by the 25
593 models during 1951-2000. For those models with multiple members, the panel is average of all
594 members of the model.

595

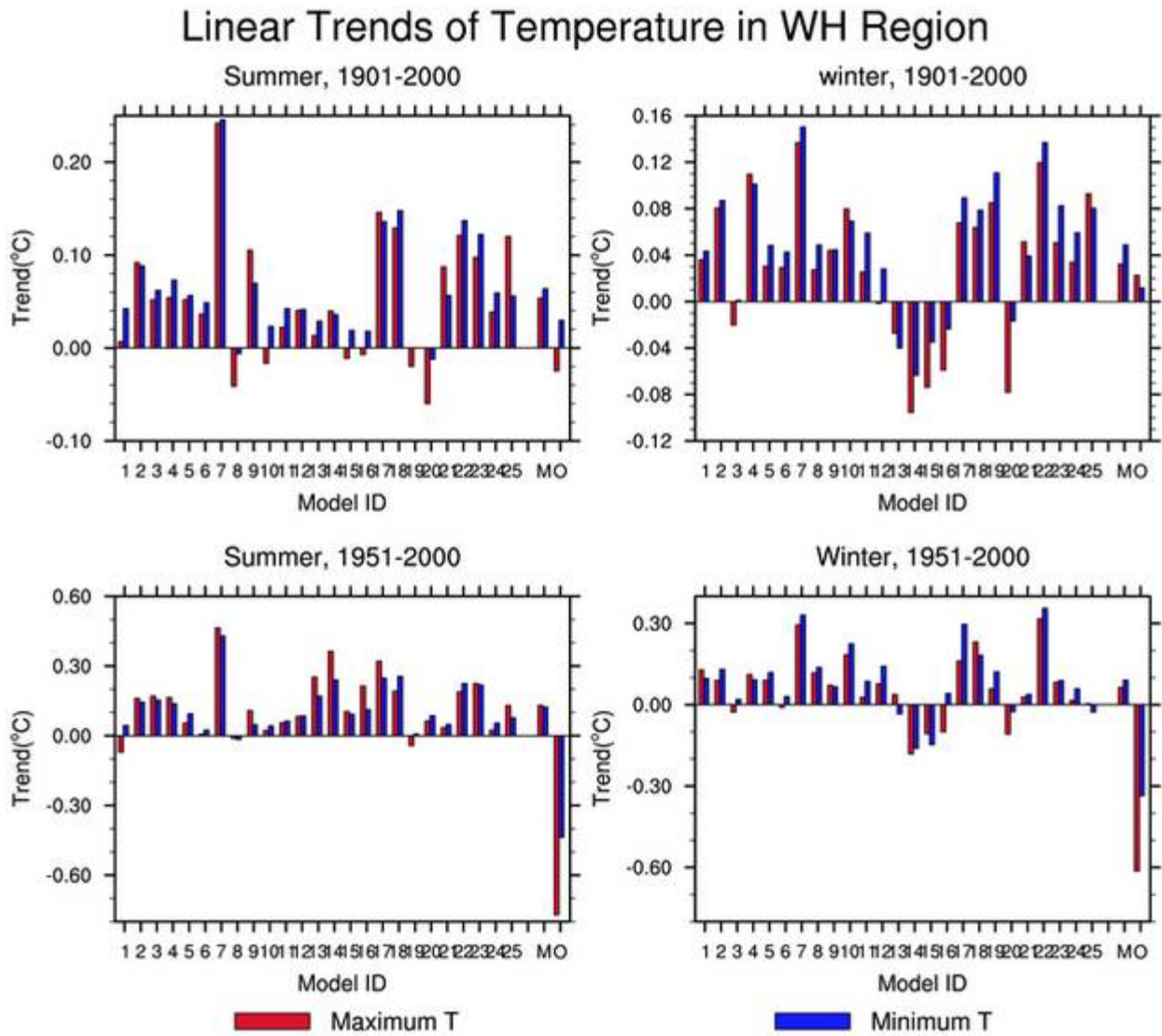


Fig. 10. Trends of Tmax and Tmin over the southeast WH in summer and winter during 1901-2000 and 1951-2000 periods. The model IDs are listed in Tab. 1. The right most two dual-bars represent all model mean (M) and observation (O), respectively.

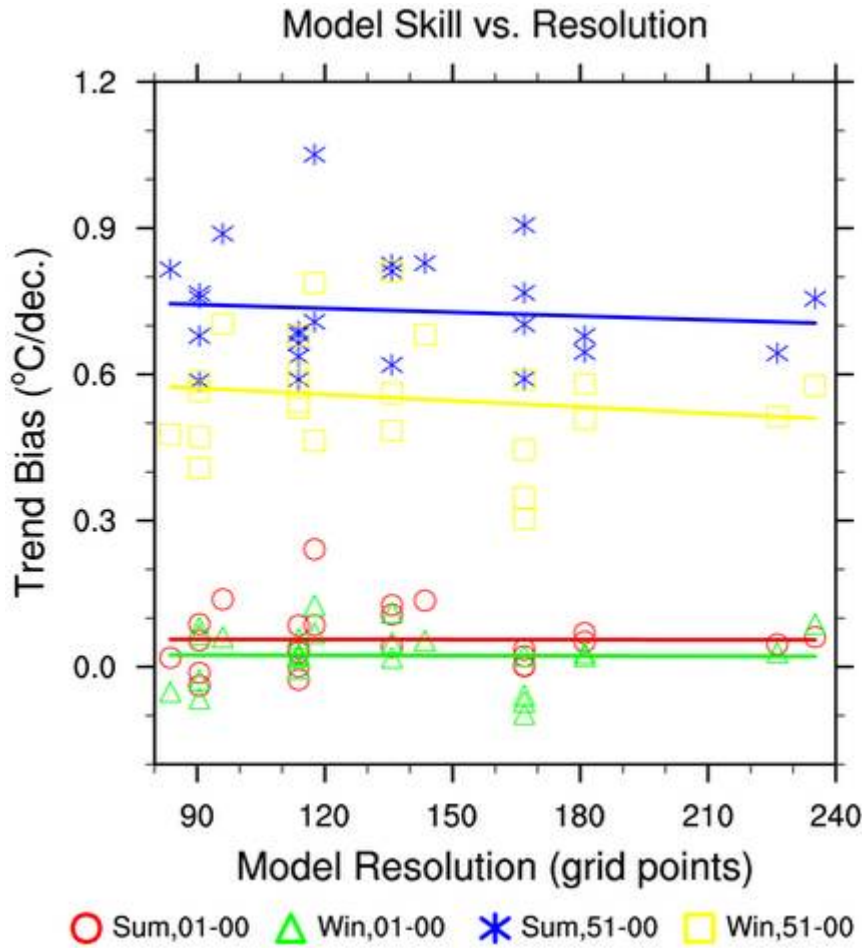


Fig. 11. Scatter plot of model biases (modeled – observed trends) versus model horizontal resolution expressed in grid points for 1901-2000 (01-00) and 1951-2000 (51-00).

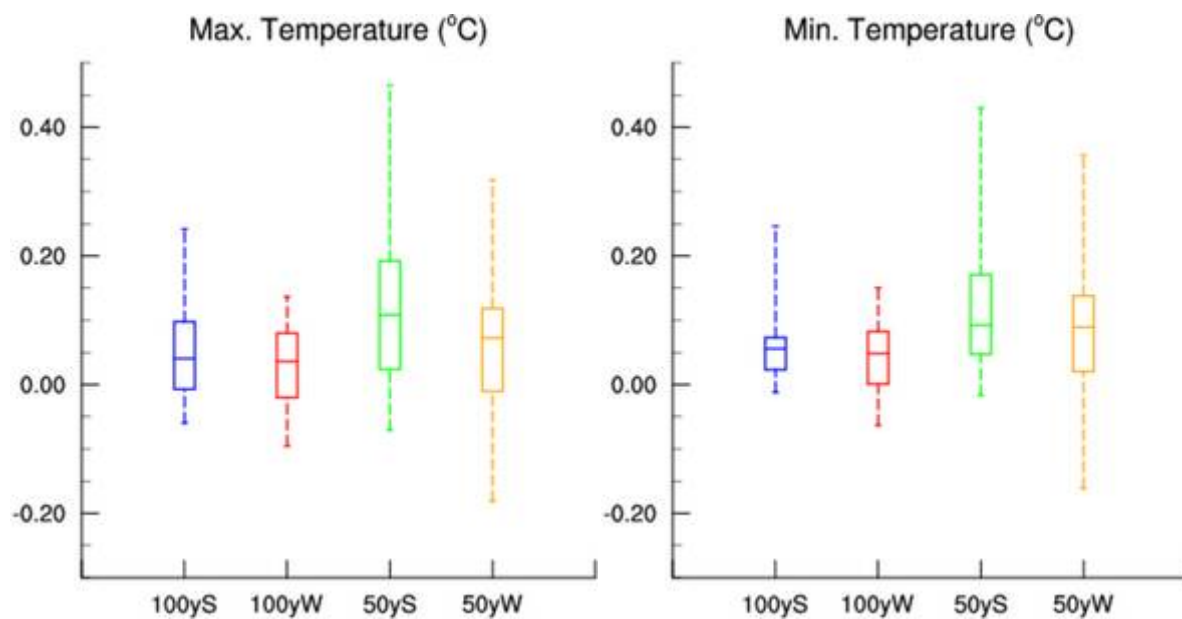


Fig. 12. Statistics of 25-model simulated southeast WH temperature trends in summer and winter during the whole and half of the 20th century. 100yS (W): 1901-2000 summer (winter); 50yS (W): 1951-2000 summer (winter).

Summer Mean Temperature Change during 1951-2000 ($^{\circ}\text{C}/\text{dec.}$)

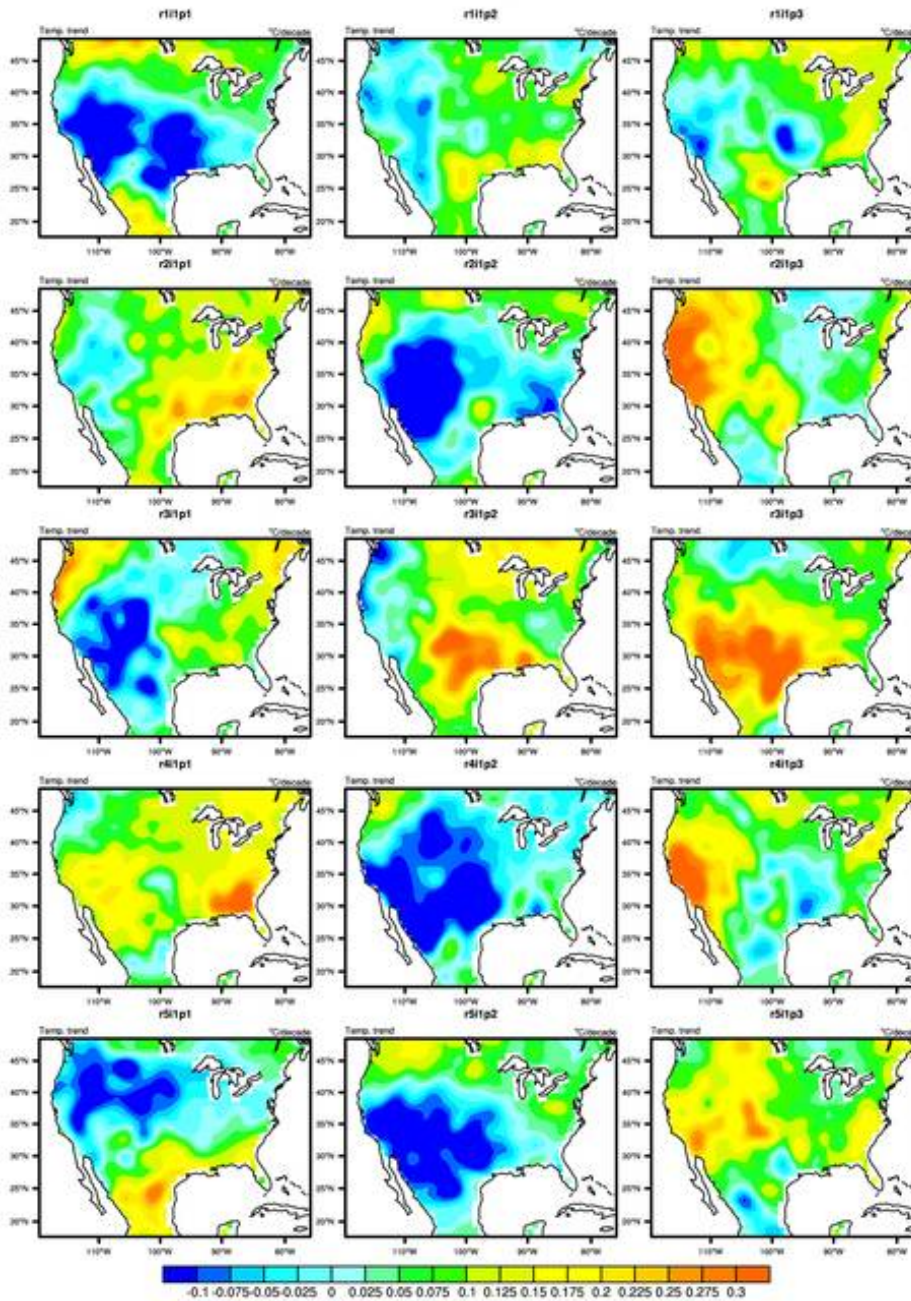


Fig. 13. Linear trends of Tmax simulated by the 15 individual members of GISS-E2-H model during 1951-2000. The triad of integers in ensemble member (i.e., panel) name rNiMpL (N, M, L) denotes initial time, initiation method, and perturbation physics, respectively.

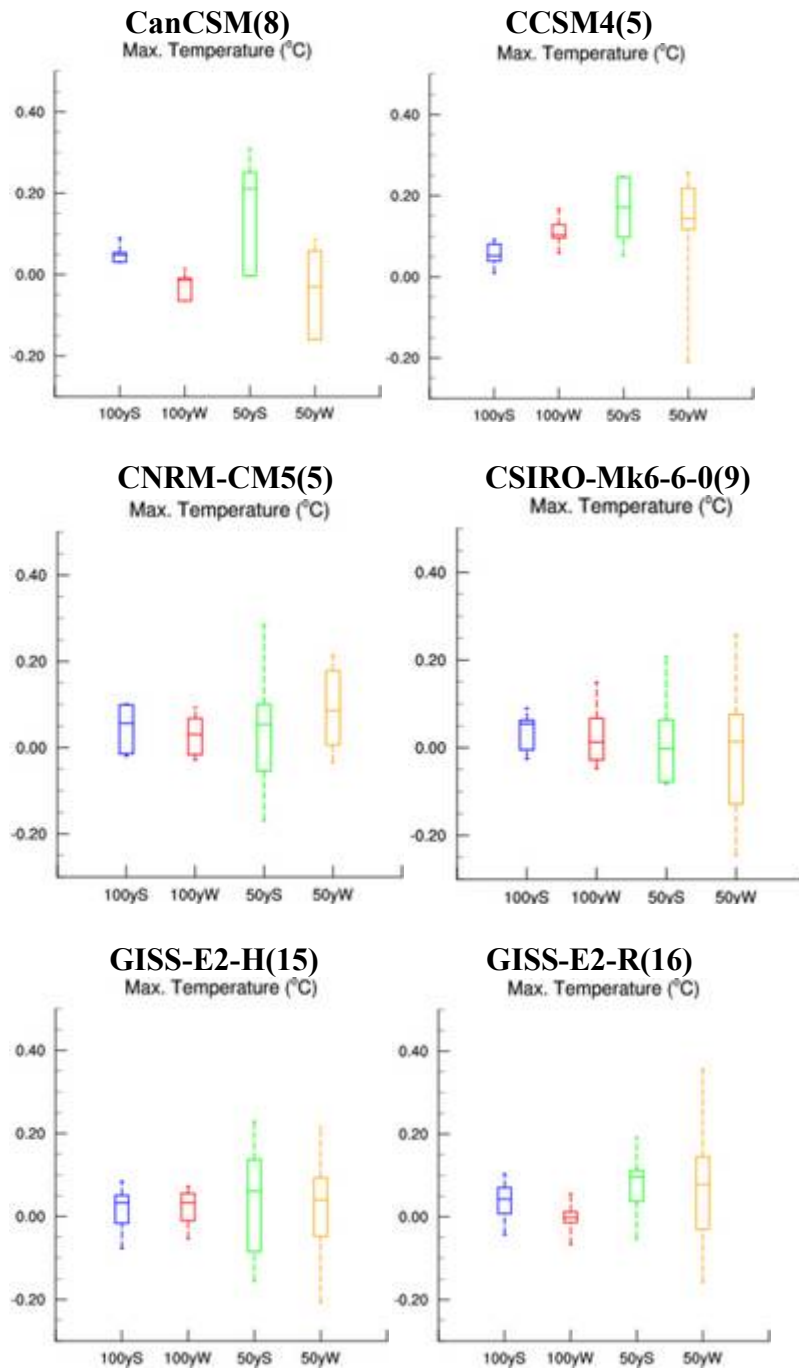


Fig. 14. Same as Fig. 12 but, for Tmax of individual models that have more than 8 ensemble members.

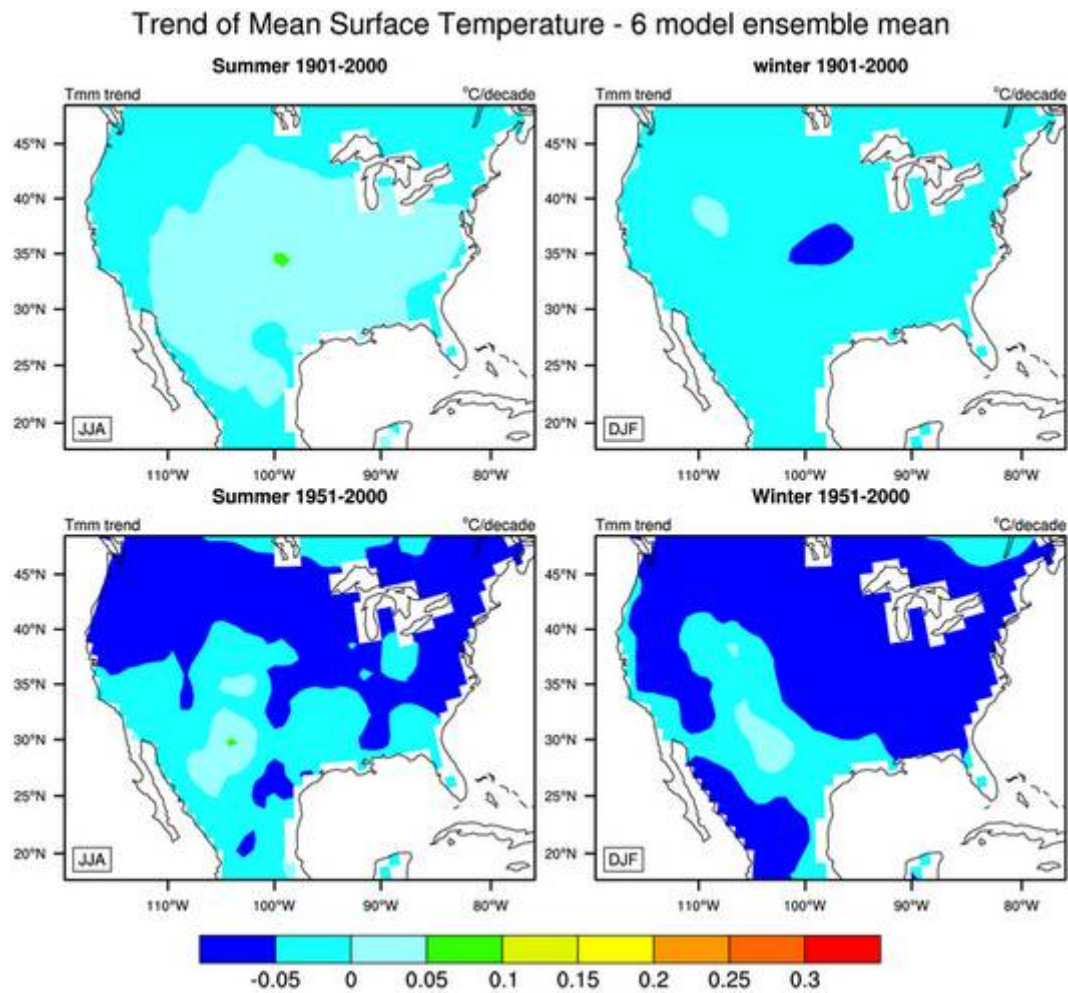


Fig. 15. Six-model ensemble mean of linear trends of Tmean simulated in the *historicalNat* experiment in summer (left) and winter (right) during 1901-2000 (top) and 1951-2000 (bottom).

Trend of Mean Surface Temperature - 6 model ensemble mean

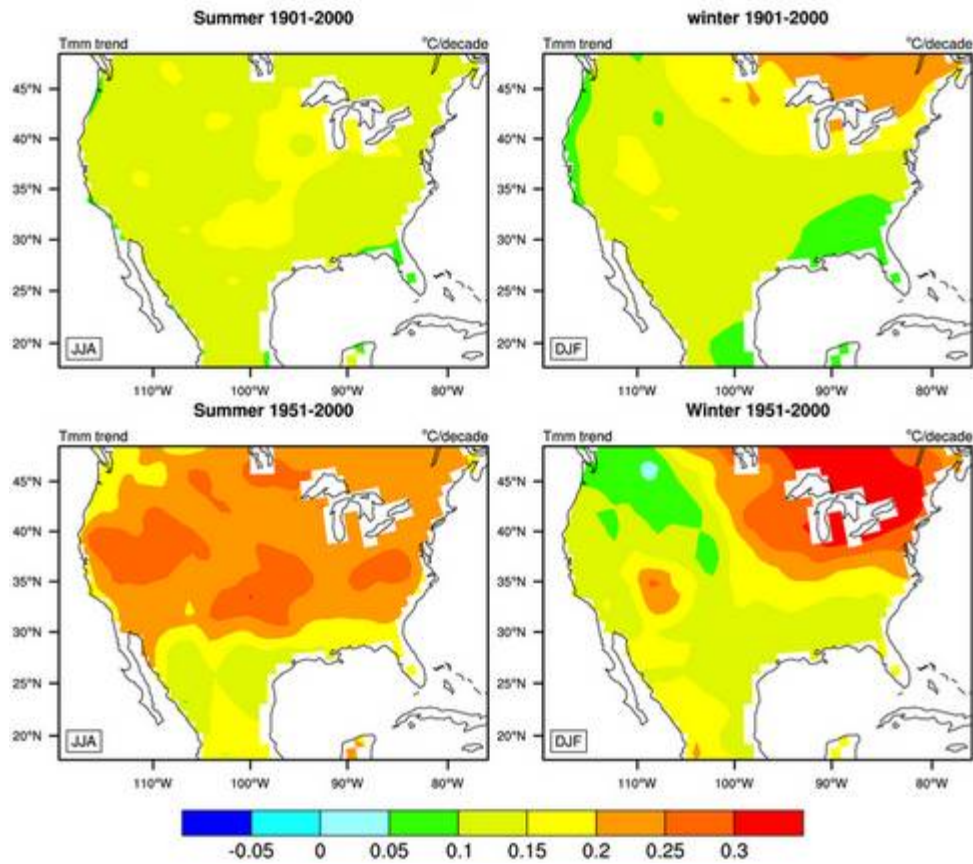


Fig. 16. Same as Fig. 15, but for *historicalGHG*.

Trend of Mean Surface Temperature - 6 model ensemble mean

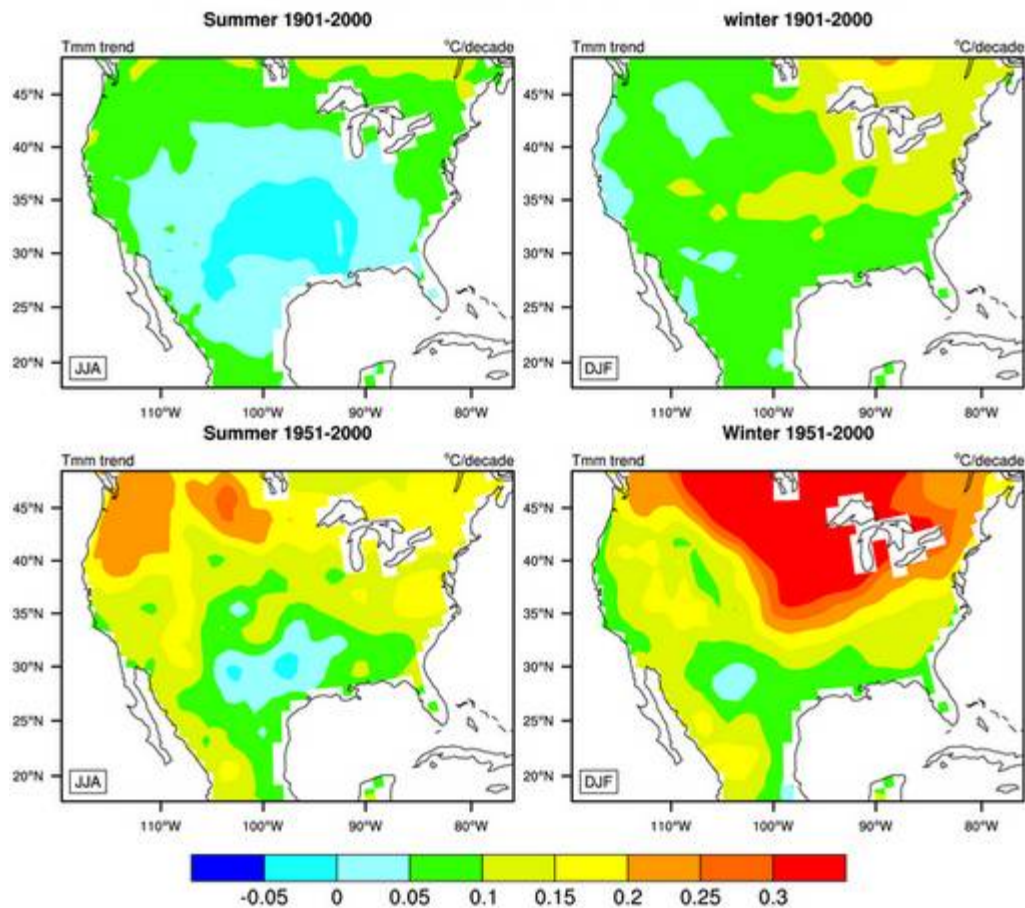
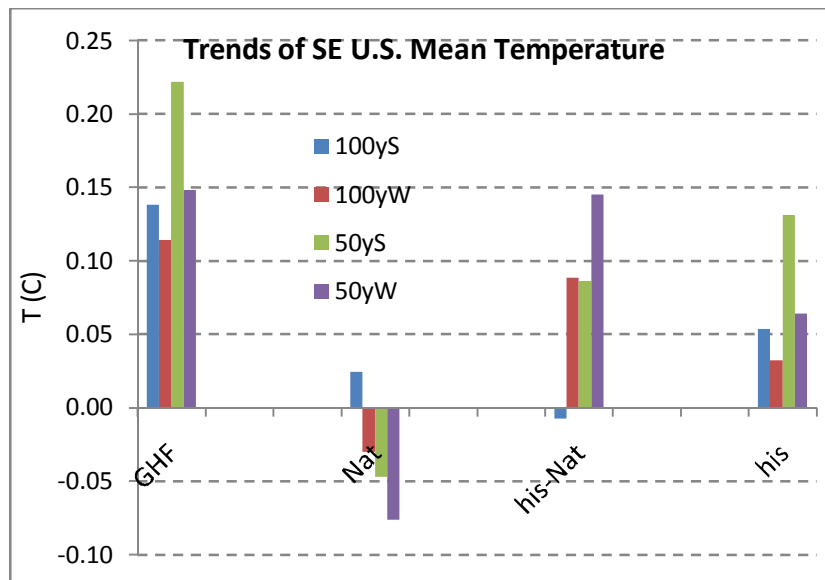


Fig. 17. Same as Fig. 15, but for the difference between all forcing (*historical*) and natural forcing only (*historicalNat*) experiments.

651



652

653

654 Figure 18. Comparison of Tmean trends in the southeast WH. under different scenarios for

655 different durations in summer and winter.

656

657

658

659

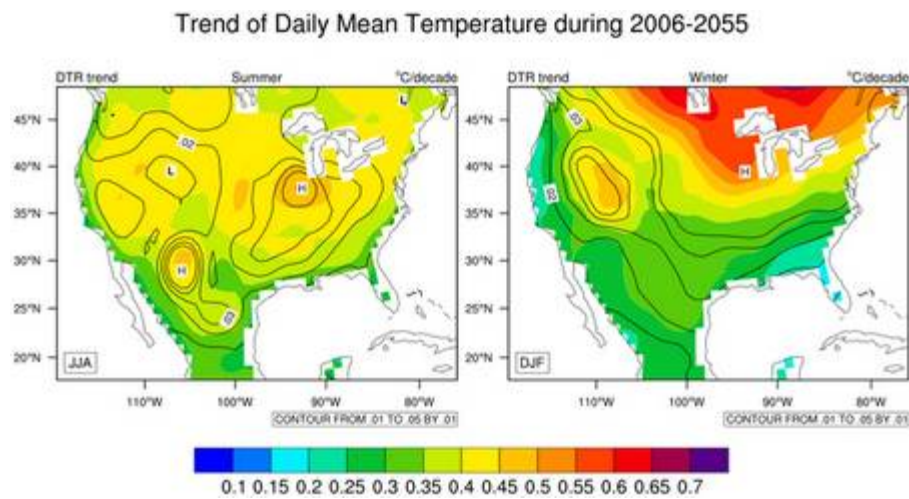
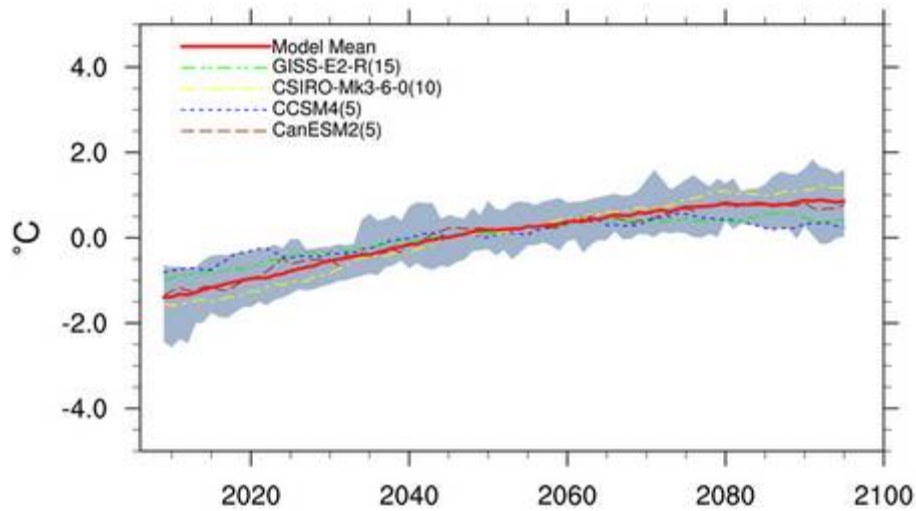


Fig. 19. Linear trend of Tmean during 2006-2055 averaged among 22 models with 63 members in *RCP4.5* experiment. The contours are the inter-model spread.

Time Series of Summer WH Mean Temperature



Time Series of Winter WH Mean Temperature

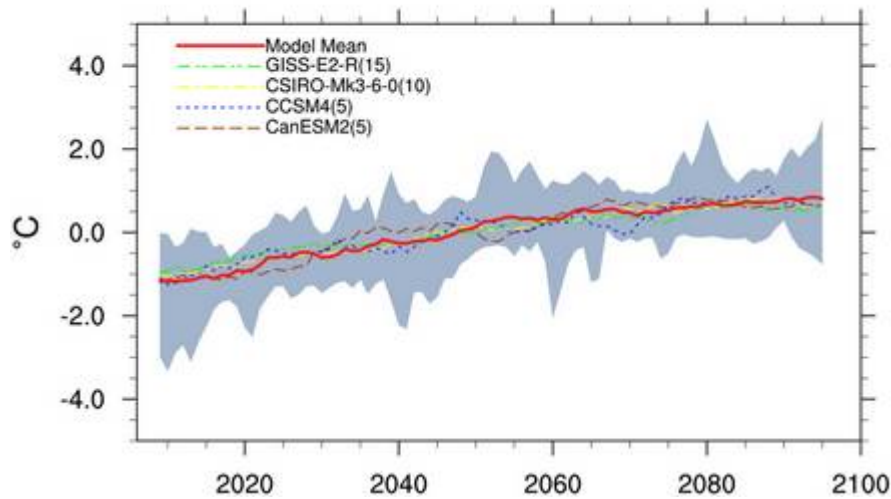


Fig. 20. Time series of Tmean in the southeast WH simulated by 22 models in the *RCP4.5* experiment. The five curves of individual models are those with largest numbers of ensemble members. The shaded areas bracket maximum and minimum values among the 22 models. The values plotted are anomalies from the 92-year mean (2006-2097) and the WH average is weighed using cosine latitude as the weight. A 7-year running mean in time was applied.

Linear Trends of Temperature in WH Region

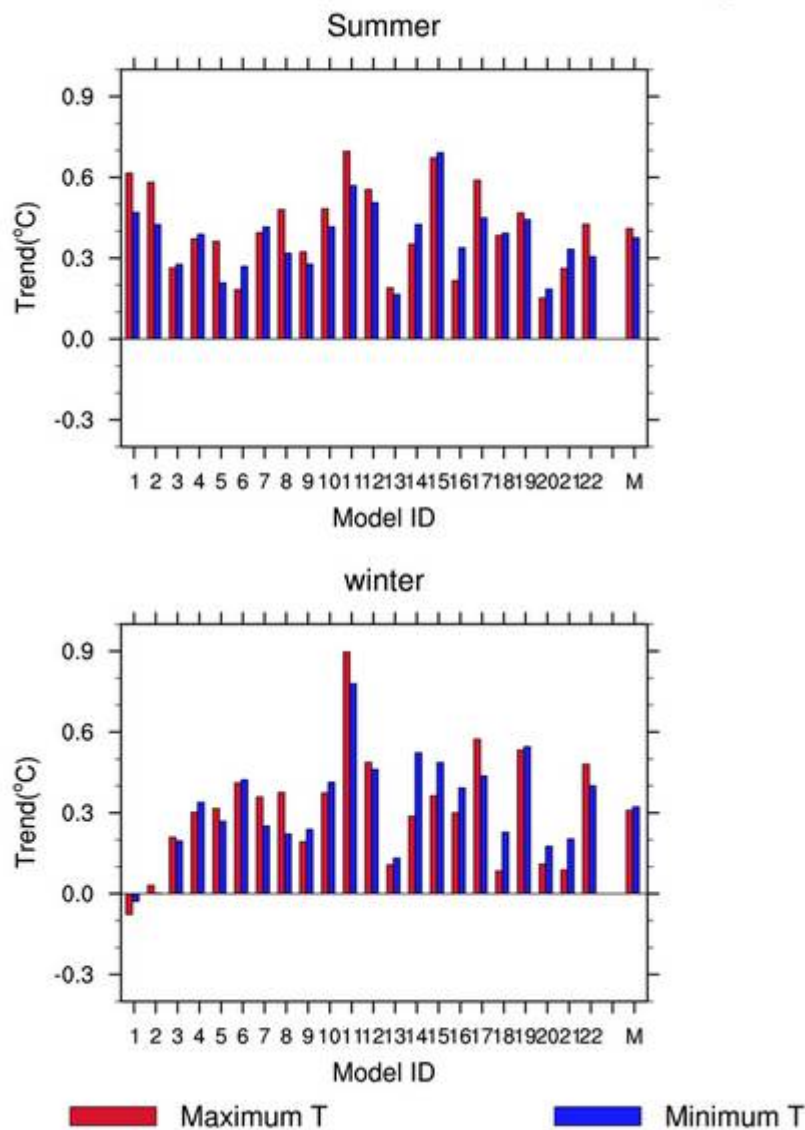


Fig. 21. Twenty-two model projected southeast WH temperature trend during 2006-2055. Model IDs are given in Table 1. The rightmost bars are the model mean.